Energy Harvesting for Nanostructured Self-Powered Photodetectors

*Lin Peng, Linfeng Hu, and Xiaosheng Fang**

Harvesting the available forms of energies in the environment to create self-powered nanosystems is now becoming a technological reality. Self-powered nanodevices and nanosystems are expected to play a crucial role in the future development of nanotechnology because of their specific role in fundamental studies and nanotechnological applications, mainly due to their size-dependent properties and independent, sustainable, maintainance-free operation. As a new field in self-powered nanotechnology-related research, self-powered photodetectors have been developed which exhibit a much faster photoresponse and higher photosensitivity than the conventional photoconductor-based photodetectors. Herein, the energy-havesting techniques are discussed and their prospects for application in self-powered photodetectors are summarized. Moreover, potential future directions of this research area are highlighted.

1. Introduction

The goal of nanotechnology is to build nanodevices that are intelligent, multifunctional, exceptionally small, extremely sensitive, and have a low power consumption. With the use of nanomaterials and nanofabrication technologies, a nanosensor device is expected to be small in size and low in power consumption; thus, it is possible to use the energy harvested from the environment to power such a system for wireless and self-sustainable operation.[1–7] Self-powered nanotechnology aims at building a self-powered system that operates independently, sustainably, and wirelessly. It is highly desired for wireless devices and even required for implanted biomedical systems to be self-powered without using a battery, which not only can largely enhance the adaptability of the devices but also greatly reduce the size and weight of the system. Therefore, it is urgent to develop self-powered nanotechnology that harvests energy from the environment for self-powering these nanodevices.

Self-powered nanodevices and nanosystems have been researched recently, and attract lots of attention due to their various advantages.[8–17] As a new field in nanotechnology-related research, nanostructural photodetectors (PDs) that can convert light into an electrical signal are crucial for wide application in many fields such as imaging techniques, light-wave communications, and so on.[18–23] The physical mechanism of photodetection is the generation of electron–hole (e–h) pairs through the optical absorption of incident photons. The photogenerated e–h pairs are then separated and collected by the external circuit by an electric field. High-performance PDs with fast speeds and low power consumption are highly desired for applications of optoelectronic integration. Due to their unique properties in electrical transport and light absorption, 1D inorganic nanostructure semiconductors such as nanowires (NWs), nanoribbons (NRs), and nanotubes (NTs) are promising candidates for high-performance PD applications.[24–28] In comparison with PDs based on traditional thin-film and bulk materials, PDs made from 1D semiconductor nanostructures usually have the advantage of higher responsivity and photoconductivity gain because of their high crystallinity, high surface-to-volume ratio, and the largely shortened carrier transit time in the reduced dimensions of the effective conductive channel.[29–31] Many semiconductors such as ZnO, TiO_2, SnO_2, ZnS, Nb_2O_5 and GaN, have been investigated to fabricate various optoelectronic nanodevices in the past several decades.[32–40] For instance, we have successfully developed an ultraviolet-A (UV-A) light PD.[41] The PD is based on a binary ZnS/ZnO biaxial nanobelt and exhibits tunable spectral selectivity and wide-range photoresponse for the UV-A band. More importantly, the optimized performance of the ZnS/ZnO-based PD is much better than that of pure ZnS or ZnO nanostructures. This research demonstrates that the 1D nanostructure PDs based on photoconductivity are excellent candidates for application, which exhibit very high on/off ratios between photoresponse current and dark current due to their large surface area-to-volume ratio and high-quality crystal structure.

However, the essential drawbacks of this kind of nanostructure-based PD are a low photoresponse current, which hence requires high-precision measurement systems to detect the signal, and a long recovery time, due to the presence of a carrier-depletion layer at the nanomaterial surface caused by surface trap states. Though some efficient routes, such as integrating multiple nanomaterials and using PDs with Schottky contacts rather than Ohmic contacts, have been demonstrated to resolve these issues, these routes often lead to complicated, time-consuming, and uneconomic device fabrication processes. Most importantly, these PDs need to be driven by external batteries.

Dr. L. Peng, Dr. L. F. Hu, Prof. X. S. Fang
Department of Materials Science
Fudan University
Shanghai, 200433, PR China
E-mail: xshfang@fudan.edu.cn

DOI: 10.1002/adfm.201303367

Although a battery or energy storage unit may be a choice for powering these nanodevices, the methods will not only largely increase the system size but also greatly limit its mobility and independence for application in areas such as large-area wireless environmental sensing, chemical and biosensing, and in situ medical therapy monitoring. In this case, harvesting energy from the environment is an essential solution for building self-powered PDs, which is indispensible for sustainable operation. Compared with these traditional PDs, self-powered PDs exhibit a much faster photoresponse speed than the conventional photoconductor-based PDs. Further advancements for self-powered PDs include fast response times, high photosensitivity, good photosensitivity linearity in a large light-intensity range, and a large-scale, low-cost, and environmentally friendly fabrication process.[42,43] Therefore, self-powered PDs are currently attracting a great deal of interest and will hold great promise in future nano-optoelectronic devices, such as a self-powered nanoscale PD network, which is highly desired for waste-water and air-pollution monitoring systems that feature low energy consumption, low cost, and high sensitivity.[44,45]

To date, there have been many methods developed to build self-powered nanoscale PDs, which provide a great opportunity for using nanostructured materials in ways that exploit their novel properties to optimize the potential application of self-powered PDs. Here, a selection of recent work related to self-powered PDs is reviewed, with particular focus on energy harvesting of the integrated power resources and the building of a self-powered system. We begin with a detailed introduction of various methods for the fabrication of power resource devices to harvest the energies from the physical environment, then the recent efforts and great development in the building and applications of self-powered PDs are discussed. Finally, the possible challenges and opportunities that researchers face in this field are proposed.

2. Energy Harvesting for Self-Powered Nanosystems

2.1. Self-Powered Nanosystems

Generally, an integrated self-powered nanosystem includes a functional unit (such as the sensor), a power harvesting unit, an electrical measurement system, a data processing system and, possibly, a wireless communication unit (radio frequency, RF, technology).[46] Besides the sensing, data processing, transmitting, and power-harvesting components, energy storage is also an important function of self-powered nanosystems. A simply schematic view of a self-powered system is illustrated in **Figure 1**a. The energy harvester first scavenges multiple types of energy (such as solar energy, mechanical energy, chemical energy, and/or thermal energy) from the environment, then stores it in the energy storage module (e.g., capacitors), which can be used to power the other parts of the system. The sensors detect the changes in the environment, while the data processor and controller analyze the information. Then, the signal is sent out by the data transmitter, and simultaneously the response is received. Alternatively, the power-harvesting unit of a self-powered system can be utilized as both the power source and the active sensor. In this case, the functional unit of the self-powered system can not only detect the signals but also be powered by these detected signals.

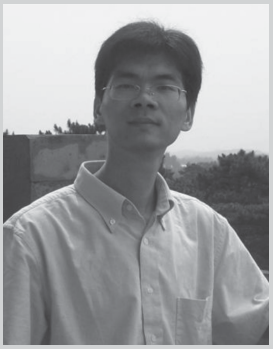

Lin Peng received his PhD from the Shanghai University in 2010. He joined in Shanghai University of Electric Power as an associate professor in 2011. He is currently a postdoctoral fellow in the Department of Materials Science, Fudan University. He current research interests include synthesis, novel properties, and applications of semiconductor nanostructures, with a special focus on nanostructured photodetectors.

Linfeng Hu received his BS and MS from Huazhong University of Science and Technology and Tsinghua University, respectively. In 2010, he earned his PhD in materials science and engineering from the National Institute of Materials Science (NIMS), Japan. He is currently an associate professor at the Department of Materials Science, Fudan University, China. His research interests include in the synthesis and self-assembly of low-dimensional nanostructures into nanofilms and nanodevices with novel properties.

Xiaosheng Fang received his PhD from the Institute of Solid State Physics, Chinese Academy of Sciences in 2006 under the supervision of Professor Lide Zhang. He joined NIMS, Japan as a JSPS postdoctoral fellow and then the ICYS-MANA as a researcher. Currently, he is a professor at the Department of Materials Science, Fudan University, China. His current research topic is the controlled fabrication, novel properties and optoelectronic applications of semiconductor nanostructures, especially with a focus on II–VI inorganic semiconductor nanostructure-based photodetectors.

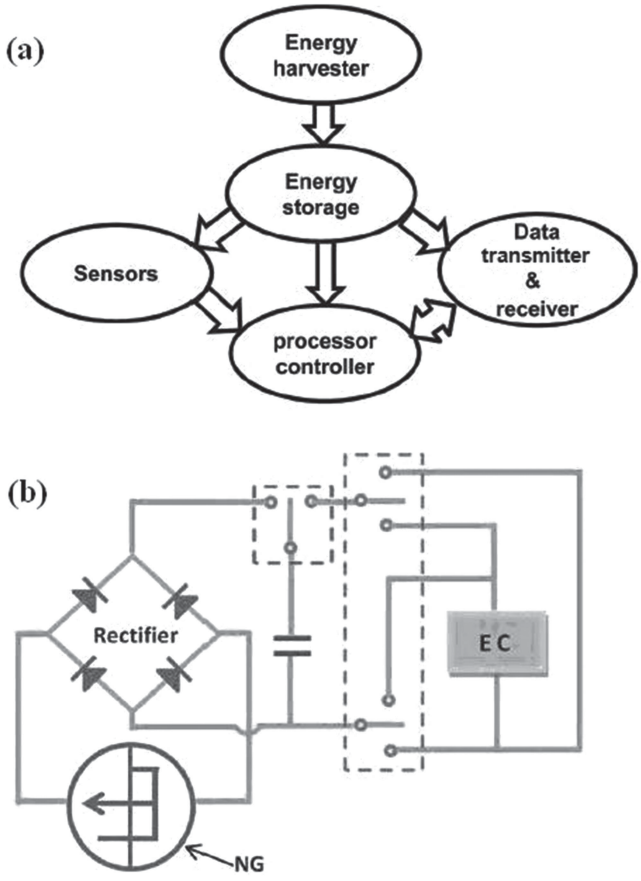

Figure 1. Schematic diagram of a self-powered system. a) An integrated system can be divided into five modules: energy harvester, energy storage, sensors, data processor & controller, and data transmitter & receiver. Reproduced with permission.[46] Copyright 2011, American Chemical Society. b) The self-powered electrochromic device system with an integrated NG-charged power source. Reproduced with permission.[47] Copyright 2012, Royal Society of Chemistry.

To demonstrate the operation of a self-powered nanosystem in detail, we take a self-powered WO_3-based electrochromic (EC) device driven by an nanogenerator (NG) as an example.[47] In the self-powered EC system, the power source unit has an NG and a full-wave bridge for rectification. The NG converts mechanical energy into electricity, while the full-wave bridge transforms alternating current from the NG into unidirectional current. The electricity generated by the NG is rectified and stored in a capacitor and then released to drive the EC device (Figure 1b). The charging process and discharge process are controlled by a regular switch (blue dashed rectangle in Figure 1b). A mechanical vibration at a frequency of 6 Hz was applied to the NG. The voltage across the capacitor reached 4 V after being charged for 14 s. Subsequently, the capacitor was forwardly (or reversely) connected to the EC device and discharged. The electrochromic response time during the coloring process and bleaching process is even less than 10 s on the basis of 80% change of transmittance. This kind of self-powered system, by integrating an EC device with an NG, can be a candidate for monochrome self-powered displays in portable electronic devices as well as in electronic billboards.

2.2. Energy-Harvesting Devices for Self-Powered Nanosystems

Harvesting energy from the environment to power a micro-/nanodevice is of vital importance to self-powered micro-/nanosystems. The power required to drive such electronics is in the micro- to milliwatt range and so can be harvested from our physical environment. Once outputs on the order of milliwatts can be achieved, it is possible to have self-powered PDs, biosensors, environment sensors, nanorobotics, micro-electromechanical systems, and even portable/wearable electronics. As summarized in **Table 1**, the rationally designed materials and nanotechnologies have been developed for converting solar, mechanical, and chemical energies into electricity during the past years. Photovoltaic cells rely on approaches such as inorganic p–n junctions, Schottky junctions, organic thin films, and organic–inorganic heterojunctions.[48–51] Mechanical energy NGs have been designed based on principles of electromagnetic induction and the piezoelectric effect.[52,53] Microbial fuel cells can be used to convert the chemical energy of glucose and oxygen in a biofluid into electricity.[54] Innovative approaches have also been developed for conjunctional harvesting of multiple types of energies by using an integrated structure/material, and then the energy resources can be effectively and complimentarily utilized whenever and wherever one or all of them are available.[55–58]

2.2.1. Micro-/Nano Solar Cells

Solar cells are attractive candidates for clean and renewable power. With miniaturization, they might also serve as integrated power sources for self-powered nanosystems. The use of nanostructures or nanostructured materials represents a general approach to reduce both cost and size and to improve efficiency in photovoltaics (PVs). Semiconductor NWs have a lot of advantages as candidates for photovoltaic applications[59,60] due to their large surface-to-volume ratio, better charge collection, and the possibility of enhanced absorption through light trapping. At the same time, a NW-based PV has great application in flexible power sources compared to bulk materials.[61]

The p–n (or p–i–n) junction is an alternative structure for the PV device. Solar cell devices composed of radial p–n junctions, axial, and coaxial p–n Si nanowires (SiNWs) with efficiencies of ~0.63%, 0.5%, and 3.4%, respectively, have been fabricated as well.[62,63] A conversion efficiency of 42.3% was achieved by combining multijunction cells and concentrator technology.[64] The Schottky junction is another alternative structure for the NW-based PV device. Basically, any semiconductor can form a Schottky junction with a certain metal if their work function difference is big enough, and the carrier density of the semiconductor is low or moderate. In addition, the fabrication of Schottky junctions has the merits of low-cost and simplicity. For instance, Kelzenberg and co-workers reported a single SiNW rectifying junction solar cell with an energy-conversion efficiency of ~0.46%.[65] By using a Pt-SiNW-Al structure, Kim et al. demonstrated multiple SiNW (multi-SiNW)-embedded Schottky solar cells with a large photocurrent.[66] In order to increase the conversion efficiency, graphene with many exceptional properties such as high transparency, large thermal conductivity, and excellent electronic and mechanical properties

Table 1. Nanostructured energy-harvesting devices (please see the main text for definitions of acronyms).

Energy harvesting device	Power or power density	Output voltage	Current or current density	Response	Decay time	Ref.
Coaxial Si nanowires solar cell	~72 pW	0.260 V	0.503 nA	—	—	64
TENG (I)	31.2 mW/cm^3	110 V	6 μA	—	—	88
TENG (II)	—	18V	0.7 μA	—	—	120
GaN nanowire-based PENG	12.5 mW/m^2	24.95 mV	49.90 pA	—	—	97
PZT nanowire-based PENG	200 μW/cm^3	6 V	45 nA	—	—	117
PZT ribbon-based NG	~88 mW/cm^3	~2 V	~2.2 μA/cm^2	—	—	118
Single PZT nanowire PYNG	—	60 mV	—	0.9 s	3 s	130
Sb-Doped ZnO PYNG	3.2×10^4 W/mK^2	10 mV	94 nA	—	—	129
ZnO/P3HT:PCBM PENG	0.88 W/cm^3	1.45 V	6.05 A/cm^2	—	—	52
HC for DSSC and NG	34.5 μW/cm^2	0.243 V	141 μA/cm^2	—	—	137
HC for solar energy and NG	100 mW cm^2	0.55 V	9.2 mA/cm^2	—	—	138
Coaxial NWs-based PV device	—	0.532 V	3.47 nA	—	—	81
Flexible TENG	~10.4 mW/cm^3	3.3 V	0.6μA	—	—	89
A nanowire-based MFC	30 μW/cm^2	0.23 V	—	—	—	134
Optical fiber-based 3D HC	—	3.3 V	7.65 μA	—	—	142

has been adopted to optimize the solar cell devices.[67–69] Ye and co-workers reported CdSe NR/GO Schottky solar cells with an efficiency of 1.25%.[70] Xie and co-workers reported a graphene NR/multiple SiNW junction solar cell with an energy-conversion efficiency of ~1.47% under AM 1.5G illumination.[71] The efficiency can be further enhanced to 1.65% by using Au/graphene Schottky electrodes.[72] What's more, by combining with the Si wafer or SiNW array, graphene film/Si Schottky solar cells were fabricated which showed efficiencies in the range of 1.65–4.35%.[73–76]

The strain in the NWs, introduced during growth, device fabrication, and/or application, is an important issue for piezoelectric semiconductor-based PVs (e.g., CdS, ZnO, and CdTe). Epitaxial core–shell NWs grown with different materials acquire in general elastic strain as a result of a misfit between the inherent crystal lattices of the core and shell materials. Such a static and internally built strain can create piezoelectric polarization in the NW. Xu and co-workers have theoretically investigated the piezopotential created in a core–shell NW as a result of intrinsic strain[77,78] and its possibility for high-efficiency solar cells.[79,80] The lattice-mismatch induced strain in an epitaxial core–shell NW gives rise to an internal electric field along the axis of the NW. The effect can be employed to separate photongenerated e–h pairs in the core–shell nanowires and thus offers a new device concept for solar-energy conversion. Pan and co-workers[81] first experimentally demonstrated largely enhanced performance of n-CdS/p-Cu_2S coaxial NW-based PV devices using the piezo-phototronics effect when the PV device is subjected to an external strain. This piezo-phototronics effect could control the e–h pair generation, transport, separation, and/or recombination, thus enhancing the performance of the PV device by as much as 70%. The fabrication process of the coaxial CdS/Cu_2S NW-based PV device is shown in **Figure 2**a–c. These NW-based PV devices were 220 μm long and 4.95 μm in diameter and yielded a short-circuit current (I_{SC}) of 0.25 nA and open-circuit voltage (V_{OC}) of 0.26 V under a full-sun intensity (Figure 2d). The performance of this PV device was enhanced when the PV device was subjected to a compressive strain up to −0.41% (Figure 2e). This effect offers a new concept for improving the solar-energy conversation efficiency by designing the orientation of the NWs and the strain to be purposely introduced in the packaging of the solar cells, which has a bright future in the applications of flexible solar cells and self-powered technology.

The high-efficient micro/nano solar cells can be achieved by nanotechnology. However, the high efficiency of solar cells is offset by their increased complexity and manufacturing cost, which limit their application. Enormous efforts have therefore been made to develop a new generation of PV technologies that operate with enhanced efficiency at a lower cost.

2.2.2. Nanogenerators

Various types of mechanical energy sources have been scavenged by NGs, including sonic wave,[82] respiration,[83] and air/liquid pressure.[84] The advancement of NG technologies provides us with an alternate energy resource and pushes forward the investigation of self-powered systems.[11,46,85] NG-based self-powered nanosystems have been proven viable by self-powered pH sensors, UV sensors, small liquid crystal displays, commercial laser diodes, pressure/speed sensors, environmental sensors, and so on.[8,10,11,42,86] There are three typical approaches: piezoelectric,[87,88] triboelectric,[89,90] and pyroelectric NGs.[91,92] Alternatively, the NG can be used as a sensor to directly measure the magnitude and dynamic behavior of the mechanical triggering or temperature variation, which is a new type of active sensor for monitoring mechanical and thermal processes, such as vortex capture and ambient wind-velocity

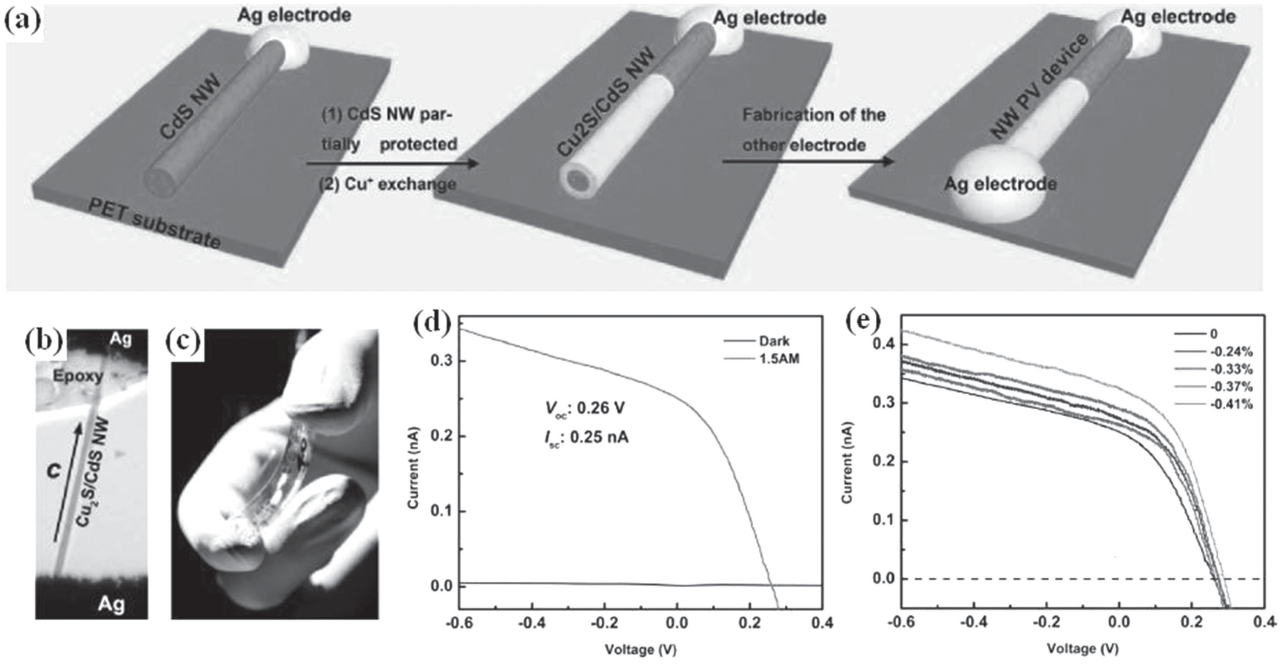

Figure 2. Fabrication and performance of the CdS–Cu_2S core–shell NW PV device. a) Schematic of the fabrication process of the PV device. b,c) Optical microscopy and digital image of a typical PV device. d) The dark and 1.5AM illuminated *I–V* curve of the NW solar cell. The insert is an optical microscopy image of the Cu_2S/CdS coaxial NW solar cell. e) The *I–V* curve of the same NW solar cell under different compressive strain, clearly indicating the current increase with increasing external compressive strain. The schematic of the measurement setup for studying the piezo-phototronic effect PV devices is demonstrated as inset. Reproduced with permission.[81] Copyright 2012, American Chemical Society.

detection,[93] low frequency vibrations,[94] automobile velocity,[95] and temperature sensing.[6] Therefore, the device can operate without external power sources; i.e., it is a self-powered system in which the NG is utilized as both the power source and the active sensor.

Piezoelectric Nanogenerators: The piezoelectric nanogenerator (PENG) converts random mechanical energy into electric energy using piezoelectric materials. The mechanism of the NG relies on the piezoelectric potential created in the NWs by an external strain: a dynamic straining of the NW results in a transient flow of electrons in the external load because of the driving force of the piezopotential.[3,96–99] The advantage of using NWs is that they can be triggered by tiny physical motions, and the excitation frequency can be just one to thousands of Hz, which is ideal for harvesting random energy in the environment. In addition, due to their small size, NGs can be effectively integrated with nano/microscale functional devices to form self-powered nanosystems.

Many piezoelectric materials, such as ZnO,[1,100] InN,[101] ZnS,[102] lead zirconate titanate $PbZr_{0.52}Ti_{0.48}O_3$ (PZT),[103–106] $BaTiO_3$[107] and polyvinylidene fluoride (PVDF)[108–110] have been used for fabricating NGs. Currently, the most popular structure is the ZnO-based NG for three reasons. First, ZnO NWs can be easily grown in large quantities by using a vapor–solid process or chemical approach at low temperature. Second, they are biologically compatible and environmentally friendly. Third, they can be grown on a substrate with any shape. ZnO NWs are unique in their suitability not only for the fabrication of nanosensors,[111,112] but also for scavenging mechanical energy.[1,87,113] In 2007, Wang and co-workers developed a direct-current PENG based on vertically aligned ZnO NW arrays, which relies on a zig-zag top electrode. This acts like an array of atomic force microscopy tips that force the NWs to bend in response to the external mechanical agitation caused by an ultrasonic wave.[87] In late 2010, Xu and co-workers presented innovative and much improved steps towards achieving a high-power-output, alternating-current NG based on vertically or laterally aligned ZnO NW arrays in which there are solid bonds/contacts between the electrodes and the ends of the NW.[42] A periodic, low-frequency, uniaxial strain is applied to the ZnO NWs by an external mechanical action to create a piezoelectric potential along the NWs, which results in an alternating electrical output. A three-layer integration of the vertical NW array integrated NG (VING) enhances the output voltage up to 0.243 V. In addition, a multiple lateral-nanowire-array integrated NG has also been fabricated by combining a rational chemical growth with novel nanofabrication. A maximum voltage output of 1.26 V has been generated by integrating 700 rows of lateral ZnO NW arrays. Furthermore, the integration of a VING with a ZnO NW-based pH or UV nanosensor has successfully demonstrated the feasibility of the independent and sustainable operation of a nanosensor using a VING with an output voltage of 20–40 mV.

The integration of flexibility to a NG has received increasing interest for realizing energy-harvesting systems in practical life. Recently, ZnO nanomaterial-based flexible NGs have been demonstrated by using elastomeric substrates. For instance, a transparent and flexible nanogenerator (TFNG)[95] has been

fabricated by exploiting flexible polydimethylsiloxane (PDMS) substrates for the growth of ZnO nanowires. With the strain of 0.12% at a strain rate of 3.56 $\%s^{-1}$, the V_{OC} and I_{SC} of the TFNG device were measured to be 8 V and 0.6 μA, respectively, corresponding to a power density of ~5.3 mW/cm^3. This output is high enough for powering up small electronic devices. The TFNG device is robust enough and has the capability of scavenging energy under the rolling of vehicle tires on the road, and the high output performance of the TFNG device under the rolling of the wheel was quite stable. The study demonstrated the application as a self-powered sensor for monitoring vehicle speed and detecting vehicle weight.

As for materials with electromechanical coupling, some of them, such as PZT[114] and $BaTiO_3$,[115] are good piezoelectric materials with a larger piezoelectric constant, as compared to those of piezoelectric semiconductor materials. However, due to poor mechanical properties, these inorganic piezoelectric materials are brittle and difficult to manipulate for the fabrication of NGs. Recent work explores a different approach that uses the direct printing of high-quality, bulk inorganic piezoelectric thin films on wafers onto plastic substrates to produce NGs with high performance.[106,107,116] This method, based on ''top-down'' techniques including photolithographic patterning and etching of source wafers, has attracted much attention, but the high expense of the facility and the low efficiency have limited its practical application. Thus, exploring a general, high-efficiency, simple, and low-cost method to fabricate aligned high piezoelectric coefficient NWs is necessary and very important for flexible and wearable NGs. In this case, a suspending sintering technique of electrospinning NWs has been developed to fabricate a flexible, dense, and tough PZT textile composed of aligned parallel NWs.[117] This textile was transferred onto a thick PET film and chemical fabric to make flexible and wearable NG. The maximum output voltage and current reached 6 V and 45 nA, respectively. This kind of NG was demonstrated to light a commercial LCD and power a ZnO NW-based UV sensor to detect UV light quantitively. In addition, integration of graphene films to PZT NW-based NGs has been achieved (**Figure 3**a–c).[118] The high efficiency, semi-transparent PZT NW-based NGs integrated with graphene films that possess outstanding mechanical and optical properties can offer unique benefits in high-performance flexible and transparent devices. The NGs showed a high output voltage of ~2 V, a current density of ~2 μA cm^{-2}, and a power density of ~88 mW cm^{-3} at an applying force of 0.9 kgf (Figure 3d,e). This can efficiently run commercially available electronic components in a self-powered mode, without any external electrical supply.

Triboelectric Nanogenerators: The triboelectric nanogenerator (TENG) is different from the PENG in design.[119] The triboelectric associated electrostatic phenomena are the most common phenomena in our daily life, from walking to driving, but have been ignored as an energy source for electricity. It will be wonderful if one can use the electric charges/potential generated by a tribological process to generate electricity. Recently, a flexible triboelectric generator using all-polymer-based materials has been developed.[119] By stacking two thin polymer films made of Kapton and polyester, a charge generation, separation, and induction process can be achieved through a mechanical deformation of the polymer films as a result of the triboelectric effect (**Figure 4**a). This is a simple, low-cost, readily scalable fabrication process for a generator that can convert random mechanical energy in our living environment into electric

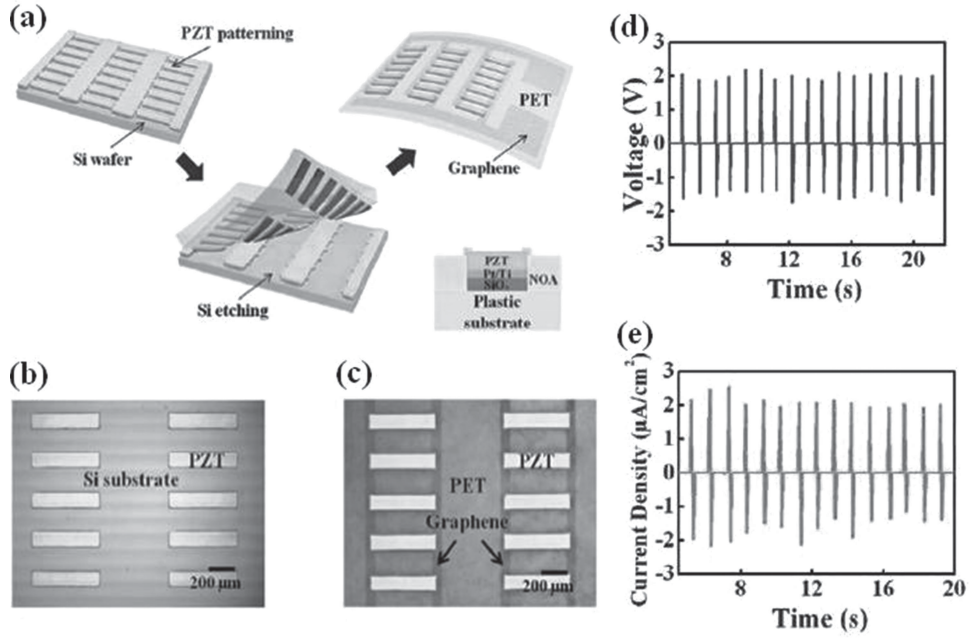

Figure 3. Schematic illustration and output measurement of a flexible PZT NG. a) Overview of the fabrication process for PZT NGs and schematic cross-sectional view. b) Optical image of PZT nanoribbons on silicon wafer. c) PZT nanoribbons with graphene electrodes on the PET film. d) The voltage and e) current density of a PZT nanogenerator with doped graphene electrodes when a dynamic load was applied on top of the NG by touch. Reproduced with permission.[118] Copyright 2012, Royal Society of Chemistry.

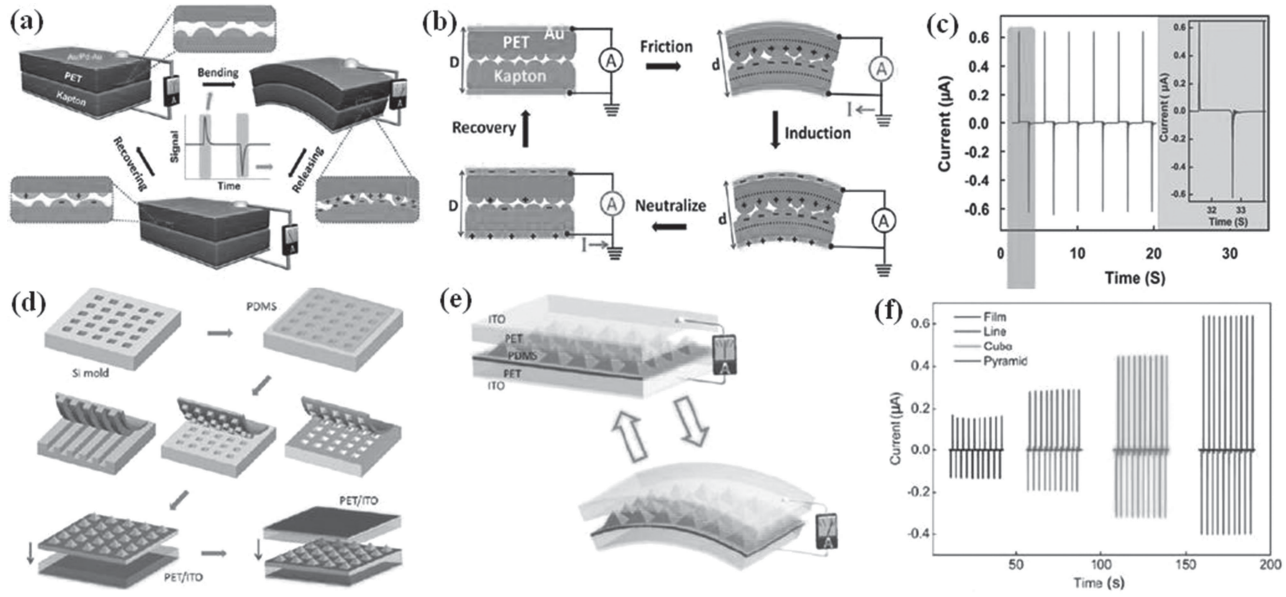

Figure 4. Schematic illustration, working principle and electric output of TENGs. a) Images of the flexible TENG and mechanical bending equipment. b) Proposed mechanism of the TENG. c) I_{SC} when forward-connected to measurement system. Reproduced with permission.[119] Copyright 2012, Elsevier. d) The patterned (100) Si wafers serve as the mold for the fabrication of a PDMS thin film with various features such as patterned lines, cubes, and pyramids. e) Schematic illustration of the charge-generating process of the triboelectric generator. f) Output current of the TFNG using a PDMS thin film with a flat surface and various patterned features. Reproduced with permission.[120] Copyright 2012, American Chemical Society.

energy using the well-known triboelectric effect. The basic principle of the triboelectric generator can be described as follows (Figure 4b): 1) The two stacked insulating polymeric materials are touched and rub each other when deformed by an external mechanical deformation. Thus, triboelectric charges with opposite signs are generated and distributed on the internal surfaces of the two polymers. 2) The opposite triboelectric charges become separated with an air gap and form a dipole moment as soon as the deformation starts to be released. As a result, an electric potential difference is established between the two planar electrodes. 3) The electrons flow from the side with lower potential to that with higher potential in order to achieve equilibrium, leading to accumulation of electrostatically inducted charges on the electrodes. 4) The dipole moment disappears or is reduced in magnitude when the deformation is then reapplied so that the two polymers are in contact. Thus, the reduced electric potential difference leads to the electrons in the electrode flowing in the opposite direction, and thus the accumulated induced charges vanish. With repeated bending and releasing of the structures, electrons are driven to flow through the external load in an alternating manner. Based on the two-layered structure, the electrical output of the triboelectric generator achieves a peak voltage of 3.3 V and a current of 0.6 μA with a peak power density of ~10.4 mW/cm^3 (Figure 4c). Triboelectric generators could harvest energy from human activities, rotating tires, ocean waves, mechanical vibrations, and more, with great application in self-powered systems. In comparison to the existing energy-harvesting methods, a triboelectric generator has several advantages. First, the entire fabrication process does not require expensive raw materials or sophisticated equipment, which would benefit mass industrial production and practical applications of the technology. Second, the device is based on flexible polymer sheets, which have manufacturability, durability, and capability of integration with other processing technologies. Third, the type of generators based on this novel principle are likely to open up new areas of research in using organic materials for energy harvesting.

Furthermore, through rational design, this mode of power generation can be developed to build a new transparent and flexible nanogenerator (TFNG) with high output.[120] Instead of using the two relatively flat polymer sheets, some patterns have been fabricated on the polymer surfaces to increase the triboelectric power output. The TFNG was composed of a sandwich structure with two ITO-coated PET membranes and a layer of patterned PDMS thin film (Figure 4d). A type of regularly and uniformly pyramid-featured PDMS pattern at the micrometer scale was achieved through a common and scalable approach. The electrical output achieved a peak voltage of 18 V and current of 0.7 μA with a peak current density of ~0.13 μA/cm^2 (Figure 4f), which is four times as high as that of the triboelectric generator using flat polymer sheets.[119] The mechanism of the triboelectric generator is to use the potential difference between the electrodes induced by a triboelectric dipole layer in a bending or releasing process, which will drive the free electrons to flow across the external load to countervail the field produced by the triboelectric changes (Figure 4e). The TFNG has potential application in touchscreens, high-definition LCDs, and other self-powered electronic displays.

Most recently, another type of self-charged triboelectric generator for harvesting mechanical energy has been demonstrated based on a coupled process of contact charging and electrostatic induction.[90] The generator has a multilayered structure.

Between two polymer layers, a cavity is formed, which is sustained by a spacer designed for the charge generation and separation processes. The generator has the virtue of highly simple fabrication/implementation, strong performance, and extremely low cost, which properly address the limitations of energy-harvesting technologies. The electrical output achieved a V_{OC} of 110 V and an I_{SC} of 6 μA with an instantaneous electric power density of ~31.2 mW/cm^3. Moreover, it can be applied as a pulsed power source for effectively electroplating uniform silver microstructures with a fine grain size. These work not only demonstrates a promising energy-harvesting technique but also greatly broadens the application of energy harvesters.

Thermoelectric Generators: The conventional thermoelectric generators (TMENGs) mainly rely on the Seebeck effect that utilizes a temperature difference across a device to drive the diffusion of charge carriers.[121–129] For instance, a TMENG based on a single Sb-doped ZnO micro/nanobelt for thermoelectric energy conversion can produce an output voltage of about 10 mV and an output current of 194 nA under a temperature difference of 30 K between two electrodes.[129] These results support the applications of single Sb-doped ZnO micro-/nanobelts in thermoelectric energy conversion and self-powered nanodevices/systems. However, the existence of a temperature difference is a must for these devices. They cannot work when the environmental temperature is spatially uniform and under a time-dependent temperature fluctuation. Recently, a TMENG based on ZnO NW arrays have been fabricated as a key technology for converting heat energy into electricity (**Figure 5**a).[91] The mechanism of TMENG is to use the anisotropic polarization in ZnO nanowires created as a result of time-dependent temperature fluctuations to drive electrons to flow. Under forward connection, a sharp negative voltage/current pulse (~5.8 mV/108.5 pA) has been observed by varying the temperature in the vicinity of the NG from 295 to 289 K (Figure 5b).

PZT nanomaterials may be another good choice for the TMENGs due to a large pyroelectric coefficient. A TMENG based on a single PZT micro-/nanowire was fabricated, which was used as a self-powered temperature sensor.[130] The output voltage of the sensor was found to linearly increase with an increasing rate of change in temperature of the detected heat sources. Under forward connection, a sharp negative voltage/current pulse (about 60 mV/0.6 nA) was observed when the temperature was increased from 296 to 333 K. The response time and reset time of the fabricated sensor are about 0.9 s and 3 s, respectively. The sensor can light an LCD when the temperature of the heat source is up to 473 K, which can be used in high-temperature early warning systems. The self-powered temperature sensor could be applied in temperature measurements in environmental sciences, safety monitoring, medical diagnostics, and more.

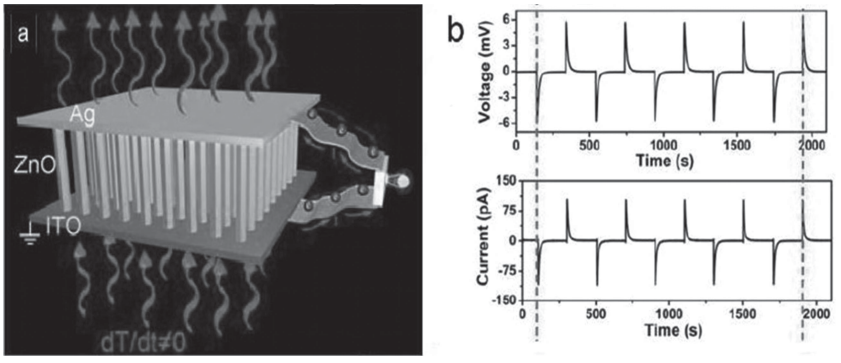

Figure 5. Schematic illustration and electric output of the TMENG. a) Schematic diagram showing the structure of the TMENG. b) Measured V_{OC} and I_{SC} of the TMENG at forward connection to the measurement system, when it was subject to a repeated temperature change from 295 to 289 K. Reproduced with permission.[91] Copyright 2012, American Chemical Society.

2.2.3. Micro Fuel Cells and Biofuel Cells

Fuel cells have many advantages over conventional batteries, including more rapid recharging and much higher energy storage density.[131] It is expected that fuel cells of sizes in the nanometer range will be accomplished eventually. Pan and coworkers presented the first micrometer-sized fuel cell using Nafion/poly(vinyl pyrrolidone) (PVP) nanowires (NPNWs) as the electrolyte.[132] The micro fuel cell (MFC) was monolithically integrated on a silicon substrate and consisted of NPNWs, PtRu/C and Pt/C catalysts, two outleading electrodes, methanol as fuel, and air as an oxidant (**Figure 6**a,b). For the best output of the developed MFC, the V_{OC} was 0.43 V and the current density and maximum power density were approximately 4.33 μA/μm^2 and 0.44 μW/μm^2, respectively, at 333 K (Figure 6c). These results showed that the performance of the MFC was several orders of magnitude higher than that of traditional fuel cell power sources.[131] Furthermore, it is revealed that the proton conductivity of NPNWs showed a very strong increase with decreasing diameter of the NPNW: the proton conductivity could be enhanced by orders of magnitude when using NPNWs with a diameter of less than 2.3 μm. The power generated by a single 2.1 μm NPNW-based micro fuel cell was about 1.54 μW, which is enough to drive low-power-consuming complementary metal-oxide semiconductor (CMOS) circuits and certain nanodevices.[132,133] Though the power generated by a single NPNW-based MFC is too small to serve as a power source for portable electronics like a personal digital assistant, this limitation could be overcome by increasing the number of the nanowires. NPNW-based MFC would provide a great future for integrated, self-powered nanodevices.

Subsequently, Pan and co-workers reported an NW-based biofuel cell (NBFC) based on a single proton conductive polymer NW for converting chemical energy from biofluids, such as glucose/blood, into electricity, using glucose oxidase (GOx) and laccase as a catalyst (Figure 6d,e).[134] By integrating an NBFC with a single NW-based pH sensor or glucose sensor fabricated using ZnO nanowire, a self-powered nanosensor is formed (Figure 6f).[135] For the glucose sensor, a rapid and obvious amperometric response was exhibited on the successive addition of glucose solution (Figure 6g,h). For the pH sensor driven by the NBFC, the current increased when the pH was increased step by step because the conductance of the pH sensor varied in different pH solutions (Figure 6i). For a carbon nanotube-based visible photon sensor driven by the NBFC, an

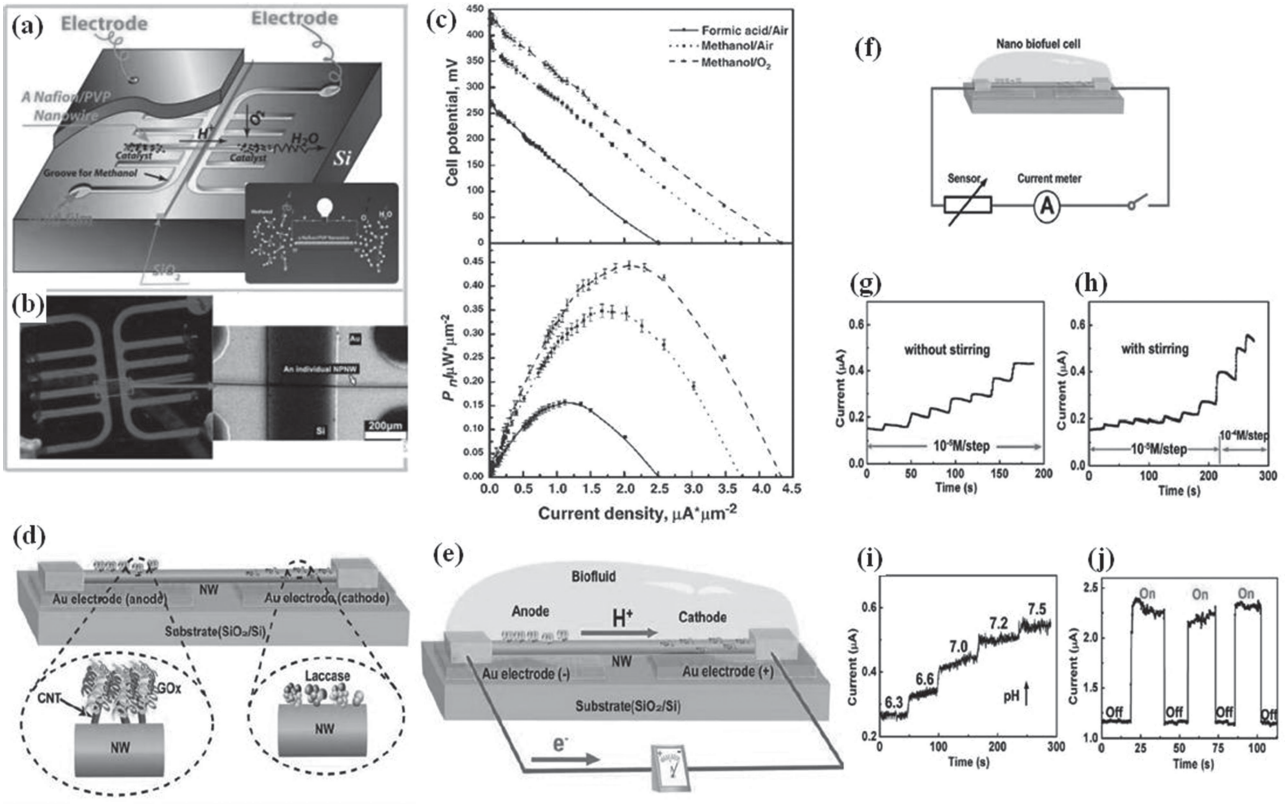

Figure 6. Schematic illustration and performance of the MFC and the NBFC. a) A groove in the Si substrate serves simultaneously as a "microchannel" fuel container and an electrode. The inset shows the working principle of MFC. b) A top-view of the micro fuel cell and a magnified image of the area marked by the red rectangle. c) Current–voltage characteristics (upper graph) and current–power density characteristics (lower graph) measured at 333 K for various fuel/oxidant combinations. Reproduced with permission.[132] Copyright 2008, Wiley-VCH. d) The NW lies on a substrate, with both ends tightly bonded to the substrate and outlet interconnects. e) The NBFC is immersed in a biofuel solution, two chemical reactions occur in the anode and cathode regions, creating a corresponding chemical potential drop along the NW. f) A nanosensor and a current meter were connected in series, and the only power source for driving the nanodevice was the NBFC. g,h) Current response of a glucose nanosensor driven by the NBFC. The difference between them is that the solution in case (g) is without stirring, while that in case (h) is stirring. i) Current response of a pH nanosensor driven by the NBFC. j) A carbon nanotube-based visible light sensitive photon nanosensor driven by a NBFC in responding to the on and off of visible light. Reproduced with permission.[134] Copyright 2010, Wiley-VCH.

obvious amperometric response was presented when the light was turned on and off (Figure 6j). These studies show that the NBFC can truly serve as a power source not only for driving in vivo nanosensors, but also for other devices.

Although the MFC exhibits unique features such as long-term stability and fuel efficiency, the power densities are typically lower owing to inefficient mass transfer across cell membranes, which might limit the application of the MFC in miniaturized electronic devices. Compared with the MFC, an enzymatic BFC uses isolated enzymes which can be mass-produced readily and cheaply. The operation principle of the BFC provides a potential biocompatible and sustainable power source for micro-/nanosystems through the harvesting of biochemical energy. However, current BFCs suffer poor stability due to the limited lifetime of extracellular enzymes and their inability to fully oxidize fuels.

2.2.4. Conjunctional Energy Harvesting

Several approaches have been developed for harvesting solar, thermal, and mechanical energies, but all of the approaches are targeted at one type of energy for one type of application, while the rest of the other types of energies are wasted. In addition, the energy available for driving a system could vary from time to time and from location to location. This is especially true for solar energy and mechanical vibration energy. Solar energy, for example, is one of the important energy sources for green energy, but solar is not always available, strongly depending on time of day and weather. Mechanical vibration energy may exist in most places, but the mechanical energy available in our environment has a wide spectrum of frequencies and time-dependent amplitudes. In this case, conjunctional harvesting of energy from multiple sources available in our living environments using a single device has become highly desirable, representing a new trend in energy technologies, not only for powering personal electronics but also for future implantable sensor transmitter devices for biomedical and healthcare applications.[136] After the first NW-based hybrid cell (HC) device was demonstrated for concurrently harvesting solar and mechanical energy in 2009,[55] a number of researchers were inspired to work on developing such a technology. Since then, many HCs

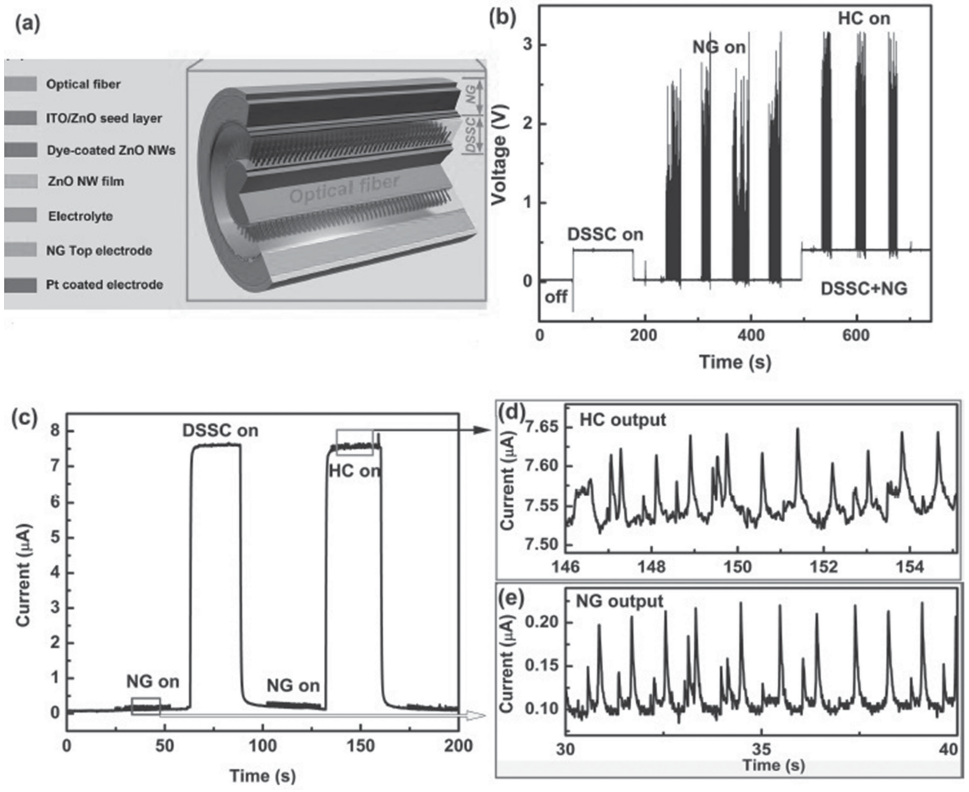

Figure 7. Design and performance of a 3D optical fiber-based HC consisting of a DSSC and an NG. a) The 3D HC is composed of an optical fiber-based DSSC with a capillary tube as counter electrode. b) *Voc* of the HC when the NG and the DSSC are connected in series, where *Voc*(HC) = *Voc*(DSSC) + *Voc*(NG). c) *Isc* of the HC when the NG and the DSSC are connected in parallel. d,e) Enlarged view of the *Isc*(HC) and *Isc*(NG), clearly showing that the *Isc*(NG) is 0.13 μA, the *Isc*(DSSC) is 7.52 μA, and the *Isc*(HC) is about 7.65 μA, nearly the sum of the output of DSSC and NG. Reproduced with permission.[141] Copyright 2012, Wiley-VCH.

for multi-type energy harvesting including solar and mechanical energy,[137,138] biochemical and biomechanical energy,[139,140] thermal and solar energy,[56] and sound and solar energy,[57] have been demonstrated. These hybrid energy-harvesting approaches can work simultaneously or individually, and they can be integrated in parallel and in series for raising the output current and voltage, respectively, as well as power.

Recently, an optical fiber-based 3D HC, consisting of a dye-sensitized solar cell (DSSC) for harvesting solar energy and a NG for harvesting mechanical energy, has been fabricated coaxially based on a traditional optical fiber as a core–shell structure.[141] The design of the DSSC is based on ZnO NW arrays grown radially around the optical fiber,[142] with the *c*-axis pointing outwards, as shown in **Figure 7**a. The conventional optical fiber is flexible and allows the remote transmission of light, which makes the DSSC suitable for solar power generation at remote/concealed locations, such as caves and basements, with applications in defensive technologies, smart construction, and environmental science. The widely available mechanical energy in our living environment will supplement the power needed when the DSSC is not available, such as at night and on rainy days. For such 3D DSSCs, light will enter the optical fiber from the end cross-section and experience multiple internal reflections inside the fiber during propagation, which will improve the performance of the DSSC. For the output of the HC, the V_{OC} of the DSSC is about 0.4 V, and the V_{OC} of the NG is about 2.9 V, resulting in a V_{OC} of the HC about 3.3 V (Figure 7b). The I_{SC} of the DSSC is 7.52 μA and that of the NG is 0.13 μA; as a result, the I_{SC} of the HC is 7.65 μA when the DSSC and the NG are connected in parallel with the same polarity (Figure 7c–e). It is noted that the output current of the HC is dominated by the DSSC, while the output voltage of the HC is dominated by the NG. Complementary contributions of the DSSC and NG are likely beneficial for the power output of the HC. The optical fiber-based HC is of great potential application for continually powering devices at remote/concealed locations.

Conjunctional energy harvesters are promising as sustainable power sources for self-powered micro-/nanosystems. However, real applications need to solve the problem of mismatching between different energy-harvesting devices, and the improvment of the conjunctional energy harvesting devices might also impart increased costs as well as difficulties in manufacturing.

2.3. Energy-Storage Devices for Self-Powered Nanosystems

Energy storage is a most important technology in the development of green, sustainable, and renewable energy sources. Green energy sources such as solar and wind energies are both

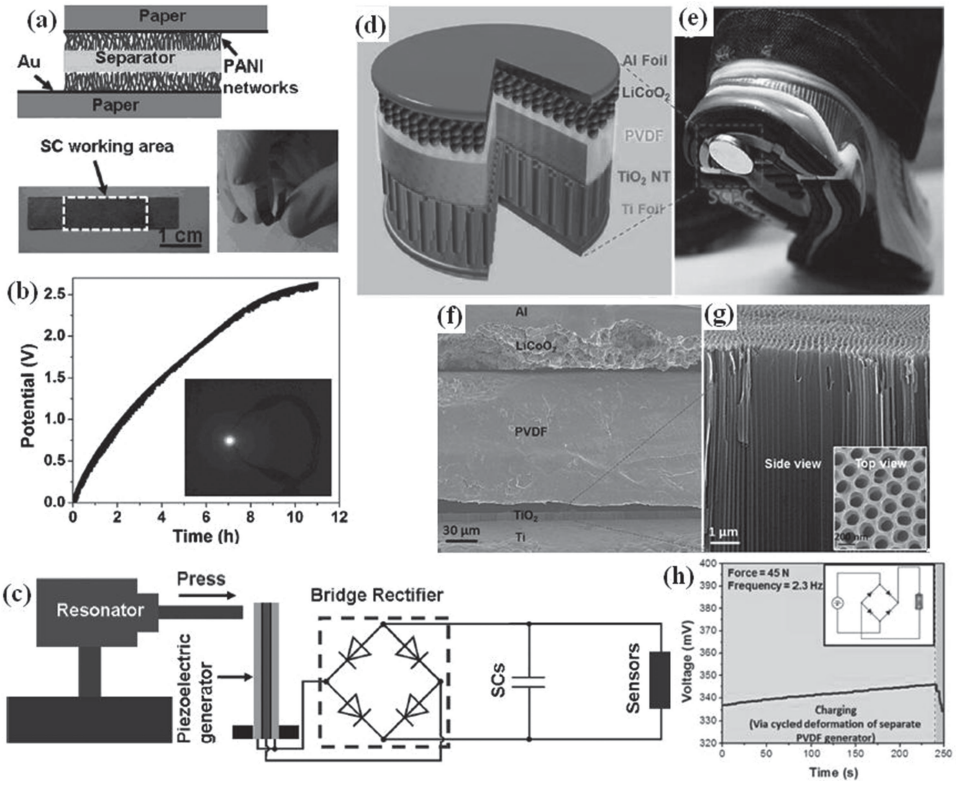

Figure 8. a) Fabricated solid-state SCs (upper) and photographs of the SC (lower). b) Charging curve for six all-solid-state SCs connected in series charged by a piezoelectric generator. The inset shows an optical image of a blue LED lighted by charged SCs connected in series. c) Schematic diagram of the self-powered nanosystems. Reproduced with permission.[155] Copyright 2012, Wiley-VCH. d) Schematic diagram showing the design and structure of the self-charging power cell (SCPC). This structure is sealed in stainless-steel 2016-coin-type cells, as shown in the inset. e) Sticking a power cell on the bottom of a shoe, the compressive energy generated by walking can be converted and stored directly by SCPC. f) Cross-sectional scanning electron microscopy (SEM) image of the self-charging power cell. g) Enlarged view of the aligned TiO_2 nanotubes. The inset is a top view SEM image of the nanotubes. h) The SCPC is separated into two individual units: a PVDF piezoelectric generator and a Li-ion battery by using PE as a separator. The inset is a schematic circuit of the traditional charging methods with separated generator and storage units connected by a bridge rectifier. Reproduced with permission.[167] Copyright 2012, American Chemical Society.

intermittent, and the harvesting of these energies may be interrupted with variances in time and space. Other energy-harvesting technologies such as NGs could easily and efficiently convert vibrational energy in living environments to electrical energy, but they cannot continuously drive small electronics because of their limited output power. Therefore, energy-storage systems are essential for providing a stable and durable output which can be regulated. Energy storage using nanomaterials is an active and important field of today's research. The main approaches to this challenge are supercapacitors[143,144] and Li-ion batteries,[145,146] both of which use electrochemical processes for storing charges using ions at a high density.

Supercapacitors (SCs), which are superior in power density, long cycle life, and fast charge–discharge rates, have demonstrated feasibility as outstanding storage components.[147–151] Compared with the SCs using liquid electrolytes, solid-state SCs have many advantages such as light weight, high flexibility, a high safety, and environmentally benign nature, which are suitable for flexible and portable electronics.[152–154] Recently, Yuan and co-workers fabricated solid-state polyaniline-based (PANI-based) flexible SCs on paper substrates as effective energy storage units for storing electric energy produced by a piezoelectric generator or a solar cell (**Figure 8**a–c).[155] The all-solid-state SC shows a power density of around 3 Wcm^{-3} at an energy density of around 0.01 Wh cm^{-3}, which is comparable to that of activated carbon SCs in aqueous electrolyte.[156] As efficient and powerful energy-storage devices, SCs could be charged and then discharge to drive various electronic components. In particular, if a sustainable and renewable energy source is used to charge SCs, they could make electronic devices work continually without a battery, forming a self-powered system (Figure 8c). The voltage of six SCs connected in series reached 2.6 V after charging for 11 h by the generator (Figure 8b), and could be charged to 3.2 V quickly in 2 min by solar cells of a higher current (around 5 mA). The charged SCs could light a blue light-emitting diode (LED) or power a strain sensor, which implies potential applications of the flexible solid-state SC in self-powered nanosystems and opens up new ways for the use of SCs.

Benefiting from its small size, flexibility, high conductivity, and large surface area, the carbon fiber (CF) can serve as a good scaffold to load active materials and fabricate small size, lightweight, and flexible SCs. For instance, the all-solid-state flexible SCs based on a carbon/MnO_2 core/shell fiber structure

were fabricated with high electrochemical performance such as high rate capability with a scan rate up to 20 Vs^{-1}, high volume capacitance of 2.5 Fcm^{-3}, and an energy density of 2.2×10^{-4} Wh cm^{-3}.[157] By integrating with a triboelectric generator, SCs could be charged and power commercial electronic devices, such as a liquid crystal displays or a light-emitting-diode, demonstrating feasibility as an efficient storage component of self-powered micro/nanosystems.

In addition, many metal oxide negative electrode materials, such as molybdenum oxide (MoO_{3-x})[158] and iron oxide,[159] show a superior capacitive performance, but the low electronic conductivity of metal oxides profoundly affects their electrochemical performance. In order to solve this problem, the use of high-specific-area and high-conductivity nanomaterials, such as ZnO and tungsten oxide (WO_{3-x}) NWs[160] as a scaffold to load electrochemically active materials, is proposed as a viable solution.[152] For instance, the MoO_{3-x}/WO_{3-x} core/shell nanostructures are grown radially on carbon fabric as a negative electrode, assembled with PANI NWs on carbon fabric as a positive electrode, to fabricate high-performance, all-solid-state asymmetric supercapacitors (ASCs) with H_3PO_4/poly(vinyl alcohol) (PVA) as the electrolyte.[148] Electrochemical measurements indicate that the fabricated ASCs can be cycled reversibly between 0 and 1.9 V. Furthermore, The fabricated all-solid-state ASCs (the volume of the whole cell was about 0.057 cm^3) exhibited a high energy density of 0.0019 Wh cm^{-3}, which is about twice that of graphene oxide (8×10^{-4} Wh cm^{-3}) and onion-like carbon SCs (1×10^{-3} Wh cm^{-3}).[156,161]

The Li-ion battery[146,162–165] is another effective energy storage approach, in which electrical energy is stored as chemical energy through the migration of Li ions under the driving force of an externally applied voltage and the follow-up electrochemical reactions occurring at the anode and cathode.[166] In general, electricity generation and energy storage are two distinct processes that are accomplished through two different and separated physical units achieving the conversions from mechanical energy to electricity and then from electrical energy to chemical energy, respectively. Recently, Xue and co-workers developed an integrated self-charging power cell (SCPC).[167] They introduced a fundamental mechanism that directly hybridizes the two processes into one, through which the mechanical energy is directly converted and simultaneously stored as chemical energy, so that the nanogenerator and the battery are hybridized as a single unit. The experimental design of a self-charging process is based on the characteristics of both piezoelectric and electrochemical properties, as schematically shown in Figure 8d–g. Under the compressive force applied to the SCPC at a frequency of 2.3 Hz, the voltage of the device increased from 327 to 395 mV in 240 s. After the self-charging process, the device was discharged back to its original voltage of 327 mV under a discharge current of 1 μA (Figure 8h). Compared with the efficiency of the traditional charging method, which is composed of a separated generator and a storage unit connected though a bridge rectifier (inset of Figure 8h), the voltage of the SCPC (65 mV) is a lot larger than that of the traditional battery. Such an integrated SCPC, which can be charged up by mechanical deformation and vibration from the environment, provides an innovative approach for developing a new mobile power source for both self-powered systems and portable and personal electronics.

To meet the pressing demands for portable and flexible equipment in contemporary society, it is strongly required to develop next-generation inexpensive, flexible, lightweight, and sustainable supercapacitor systems with large power densities, long cycle lives, and good operational safety. The primary energy storage technologies for existing designs are supercapacitors and batteries, although there are niche applications emerging for higher power density but lower energy density supercapacitors. However, the production of thin, lightweight, and flexible energy-storage devices of any type using processes scalable to commercial implementation remains challenging.

3. Self-Powered Photodetectors

Harvesting the available forms of energies in the environment to create self-powered nanosystems is now becoming a technological reality (see **Table 2**). As a new field in self-powered nanotechnology-related research, self-powered PDs have been developed. These designed self-powered PDs include two classes. One type of self-powered PD was powered by an integrated energy harvesting unit, which is usually equipped with a capacitor. This type of self-powered PD has been proven viable. At the same time, another type of self-powered PD has been developed by exploiting the photovoltaic effect. This type of self-powered PD can not only detect the signals but also be powered by these detected signals. It is highly desired that the fabricated self-powered PDs can be used to both detect the signals and produce the measurable electric energy from these detected signals.

Table 2. Nanostructured and self-powered photodetectors.

Self-powered nanostructured PD	Light	Sensitivity	V_{OC}	I_{SC}	Rise time	Decay time	Ref.
CdSe nanobelt/graphene	white	~3.5×10^5	—	0.02 μA	82 μs	179 μs	187
CdS:Ga nanoribbon/Au	510 nm	~10^3	0.16–0.18V	0.73–1.05 nA	95 μs	290 μs	175
ZnO nanowire p–n junction	UV	~10^6	~0.2 V	~0.1 μA	30 ms	50 ms	171
Opposite heterojunctions	365 nm	1.68×10^5	—	~14 μA	—	—	173
ZnO/GaN junction	367 nm	~10^6	~2.7 V	~2 μA	~20 μs	~219 μs	4
rGO-ZnO hybrid structure	white	430	—	~90 nA	<0.2 s	<0.2 s	195
Sb-doped ZnO nanobelt	325 nm	22	—	23 nA	<100 ms	<100 ms	43
PD driven by a MFC	254 nm	—	295 mV	56 nA	30 ms	40 ms	168

3.1. Self-Powered Photodetector Based on an Integrated Power Source

Generally, the type of self-powered PD with an integrated power source consists of a power unit, a light sensor, and an electrical measurement system.[14,117,140] For example, an FTNG is used to power a flexible ZnO NW-based UV sensor.[117] A voltmeter is connected with a UV sensor to measure the voltage drop on it. When the UV light is off, the resistance of the UV sensor is very large and the corresponding voltage drop on the UV sensor is about 0.2 V. When UV light is shining on the UV sensor, its resistance decreases because of the increasing carriers, and the voltage drop on the sensor decreases accordingly. With the increasing of UV light intensity, more carriers are generated in the ZnO nanowires, and the voltage drop decreases further. Therefore, by monitoring the voltage drop on the UV sensor, UV light can be detected quantitatively. The HC developed by integrating a NW-based NG with a enzyme-based BFC was also used to drive the operation of a ZnO NW-based UV light sensor.[140] The UV sensor and the HC are connected in a loop. The resistance of the ZnO NW in the HC was 7 MΩ without UV light shining on the top, and the corresponding peak voltage of the nanosensor declined 5 mV. As a result of UV radiation, NW resistance declined to 800 kΩ and the peak voltage decreased to 2.5 mV. The output difference in voltage can be used to detect the UV light illumination. Recently, a self-powered photodetector is fabricated by integrating a single-fiber NW hybrid-structured MFC with a single CdS NW-based PD in series (**Figure 9**a–c).[168] The self-powered photodetector shows an excellent response to solar light, with a response time of about 30 ms and decay time of about 40 ms. The self-powered photodetector can also be used to detect multicolored light ranging from red light to UV light. With UV light with an intensity of about 1.6×10^{-4} Wcm^{-2} shining on the CdS NW, the system current increases immediately to 1.4 nA (Figure 9d). The on–off cycles have remarkable reproducibility. The self-powered nanosystem can detect light down to a nW/cm^2 level. The responsivity for UV, blue, and green light with intensity of 2.3 $nWcm^{-2}$ of the system were 1180, 344, and 332 AW^{-1} (Figure 9e), respectively, which is two to three orders of magnitude higher than that received using a nitride based metal–semiconductor–metal PD[169] and a silicon NW-based PD.[170]

3.2. Self-Powered Photodetector Based on a Built-in Potential Difference

The self-powered photodetectors depicted above require an integrated power unit as the driving force to restrain the recombination of the photogenerated e–h pairs.[168–170] In fact, the purpose of integrating a power source is to provide a potential difference in the photoresponse nanosystem, which plays a very important role in controlling the directional movement of the photogenerated electron and hole. It is easy to understand that a potential difference in a photoresponse nanosystem is necessary for separating the photogenerated e–h pairs and forming a photocurrent. Therefore, the issue that needs to be resolved can be transferred from the power source to the potential difference, which may be easily resolved if an inner potential difference can form automatically in photoresponse nanosystem.[4,171,173,179]

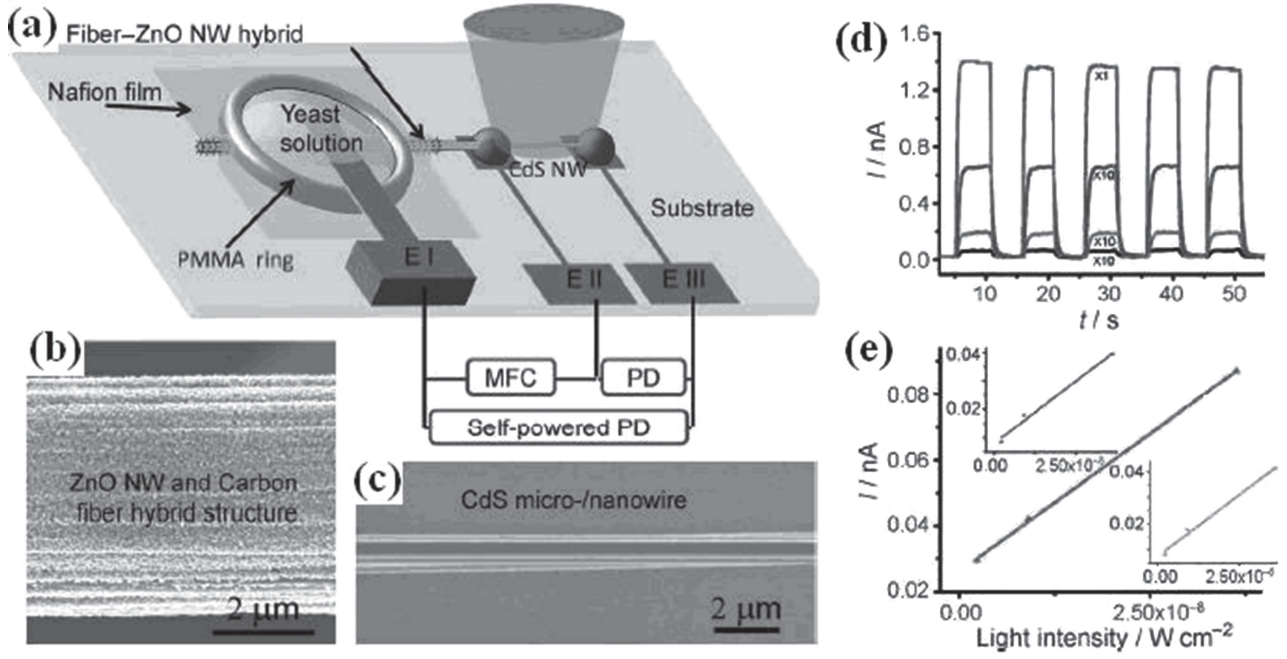

Figure 9. Experimental design and multicolor detection of the self-powered PD system. a) Illustration of a self-powered nanosystem composed of a MFC and a NW PD. E = electrode. b) SEM image of a carbon fiber covered with densely packed ZnO NWs, which was used for fabricating the MFC. c) SEM image of a CdS wire used for fabricating the photodetector. d) UV light (372 nm). e) Photocurrent as a function of the excitation intensity on the CdS NW that was illuminated by UV, blue, and green light (curves correspond to the color of the light). Reproduced with permission.[168] Copyright 2012, Wiley-VCH.

3.2.1. Self-Powered Photodetector Based on a p–n Junction

Junctions between p-type and n-type semiconductors have a built-in potential difference, so they should have the ability to provide the driving force required for the movement of photogenerated electrons and holes. In fact, photodetectors based on p–n junctions without any integrated power source have already been reported by some groups. For example, Cho and co-workers fabricated a self-powered UV photovoltaic made of a single-crystalline ZnO p–n homojunction NW device,[171] which exhibits the clear rectifying characteristics of a p–n junction diode and also shows very good UV light absorption characteristics. At a zero-voltage bias, the dark current was less than 1 pA and the V_{OC} was 0 V, whereas the photocurrent was ~1 μA and the V_{OC} was ~0.2 V under UV light illumination. Very stable and repetitive on–off cycles of the I_{SC} were observed with the light on and off. After turning off the UV illumination, the photocurrent and the output voltage immediately return to the initial levels of the dark current and open-circuit voltage. The rise time during the voltage-increasing edge and the decay time were estimated to be 30 ms and 50 ms, respectively, which are smaller than those of the previously reported photoconductive ZnO ultraviolet detectors.[172] Liao and co-workers reported an ultrafast and visible-blind UV PD based on ZnO/GaN nanoscale p–n junctions (**Figure 10**a–c).[4] The self-powered visible-blind UV PD had an ultrafast response of rise time (~20 μs) and decay time (~219 μs) (Figure 10c), which is two orders of magnitude faster than ZnO photoconductivity-based PDs. The UV PD was driven by the photovoltaic effect of the ZnO/GaN p–n junction with a short-circuit current density of up to ~5×10^4 mA cm^{-2}, a V_{OC} of ~2.7 V, a maximum output power of ~1.1 μW, and the UV photocurrent of ~2×10^{-6} A at zero bias (Figure 10b). In addition, by integrating the ZnO/GaN junction with a CdSe NW-based device, a selective multiwavelength PD was achieved (Figure 10d,e). The integrated device not only realized a self-powered red and UV detector system, but also achieved an optically operated AND gate and a multiple-state logical unit controlled by UV-light illumination.

However, these studies indicated that the photocurrent only reached the range of 10^{-6} A at zero bias. This implies that a simple junction in a nanodevice could not completely replace the external bias voltage to control directional movement of the photogenerated electron and hole. In this case, a relatively independent UV PD, based on a sandwich-like structure which is composed of one layer of p-type PANI NWs and two layers of n-type ZnO nanorod arrays, has been proposed (Figure 10f).[173] ZnO nanorod arrays were vertically grown on indium tin oxide (ITO) glass, which serves as a common substrate for directly

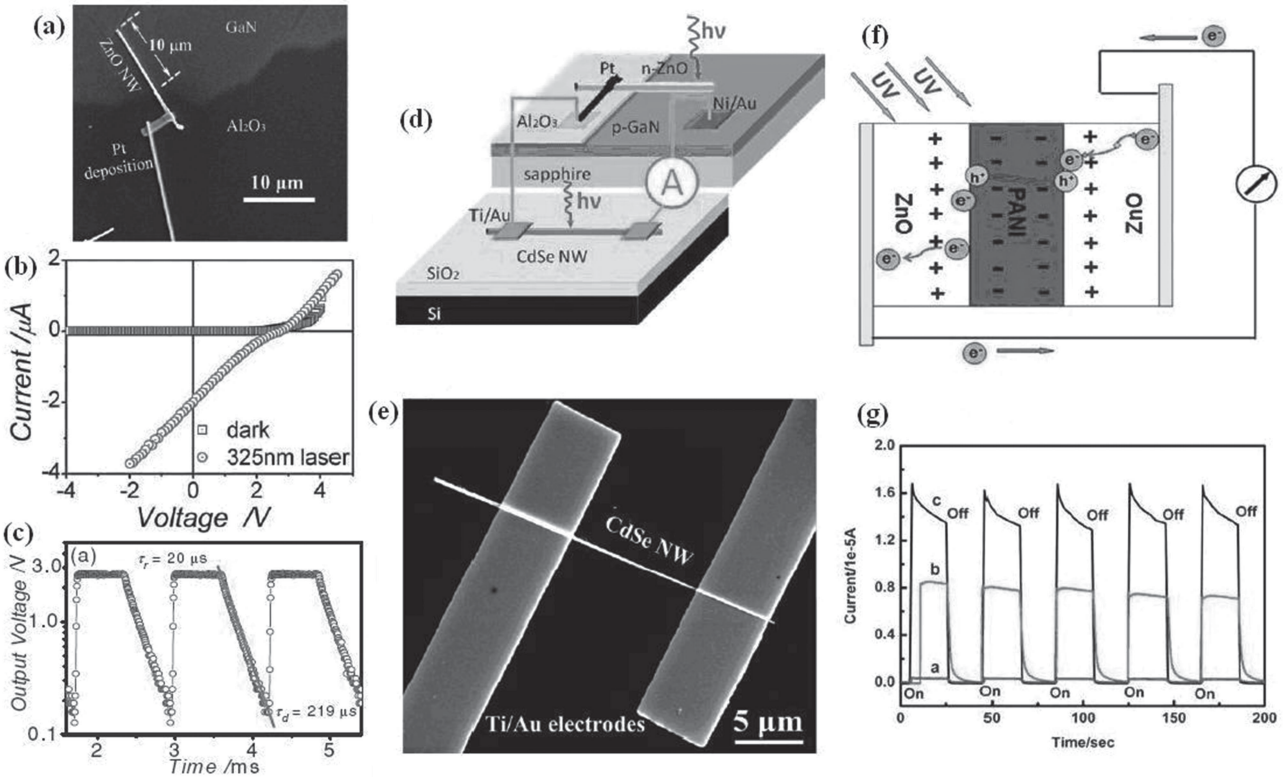

Figure 10. a) SEM image of the fabricated n-type ZnO nanowire/p-type GaN film heterojunction. b) *I–V* curves of the ZnO/GaN heterojunction under dark (square plot) and UV (circular plot) conditions. c) Photoelectrical voltage (logarithmic scale) of the ZnO/GaN heterojunction as a function of time while the incident UV light is modulated by a chopper working at 800 Hz. d) Schematic picture of the integrated PD: a CdSe nanowire device powered by an n-ZnO/p-GaN heterojunction photovoltaic unit. e) SEM image of the CdSe NW device. Reproduced with permission.[4] Copyright 2011, Wiley-VCH. f) Experimental schematic diagram of ZnO/PANI/ZnO device. g) *I–t* curves of the sandwich-structured ZnO/PANI/ZnO devices irradiated from the left side. Curves a, b, and c are for the special ZnO/PANI/ZnO device, in which the ZnO nanorods have been functionalized by PSS with 0, 1, and 5 layers, respectively. Reproduced with permission.[173] Copyright 2012, Royal Society of Chemistry.

connecting the ZnO nanorod arrays with an external circuit. Two layers of the ZnO nanorod arrays were separated by a thin layer of PANI NWs synthesized by the liquid–liquid interface method.[174] In the design, there are two opposite directional inner electric fields in the ZnO/PANI/ZnO device. A high photocurrent (~1.4×10^{-5} A) with a photosensitivity of 1.68×10^5 was observed for the special ZnO/PANI/ZnO device at zero bias (Figure 10g).

3.2.2. Self-Powered Photodetector Based on the Schottky Junction

Recent progress in PDs demonstrates that the device structure of PDs plays an important role in determining the detection ability. For instance, Ohmic contact PDs normally exhibit unparalleled performance in terms of high responsivity and high photoconductive gain, whereas Schottky junction PDs, in contrast, have advantages in sensitivity and fast response.[175–177] In addition, photovoltaic behavior usually can be observed in such Schottky-based devices, which can provide energy for themselves in applications of PDs.[176,178] This feature renders it possible to detect light irradiation without any integrated power source unit.

Zhang and co-workers presented a self-powered UV PD based on a single Sb-doped ZnO nanobelt (NB) bridging an Ohmic contact and a Schottky contact (ZnO/Au).[43] When the UV light is focused on the Schottky contact, the photon-generated electrons and holes are quickly swept away from this area in opposite directions, which can result in a photocurrent. At zero bias, the current value of the device jumped to ~23 nA and the sensitivity was found to be ~2200% under UV light illumination. The reset time of the fabricated device is less than 100 ms. Recently, a self-powered visible light PD based on a CdS:Ga NR/Au Schottky barrier diode, was investigated (**Figure 11**a).[179] The visible light PD shows the reversible switching between high and low conductance without exterior power supply when 510 nm light illumination with intensity of 0.27 mW cm^{-2} was turned on and off. The I_{on}/I_{off} ratio was ~10^3 and the response was very fast and highly stable and reproducible (Figure 11b). The mechanism of these Schottky junction PDs relies on the built-in field within the depletion region of Schottky junction. By the effective absorption of photons with energy ($h\nu$) greater than the bandgap (E_g) by semiconductor nanostructures, the electrons were driven into the CdS, and the holes were driven into the Au surface, as soon as the photogenerated e–h pairs were readily separated by the built-in field within the depletion region. The continuous accumulation of these carriers at both sides of the depletion region forms the photovoltage with a direction pointing from metal to semiconductor (Figure 11c). Once the Schottky junction is short-circuited (Figure 11d), the photogenerated carriers can transit through the external circuit, giving rise to a short-circuit current.

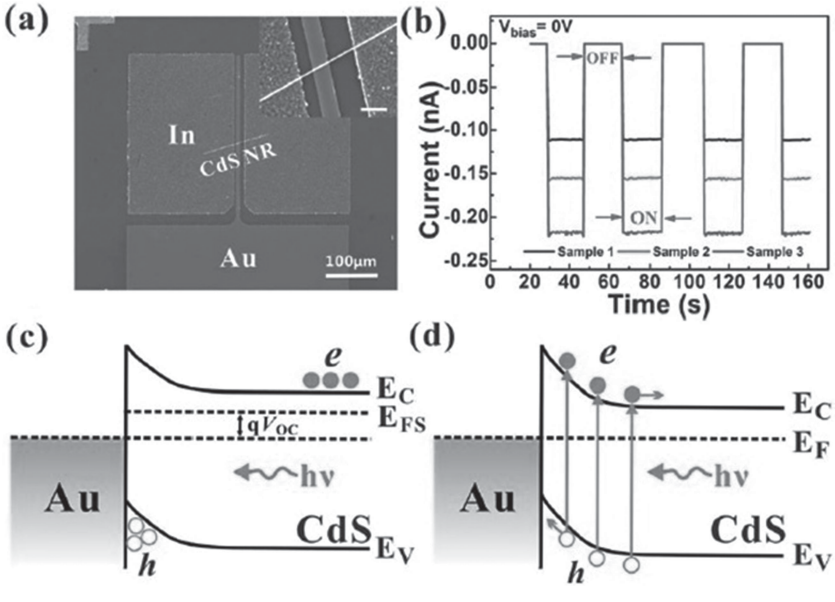

Figure 11. a) SEM image of CdS NR/Au Schottky diode. Inset shows an enlarged SEM image, the scale bar is 10 mm. b) Time response of CdS:Ga NR/Au SPDs at zero bias under light illumination of 510 nm with intensity of 0.27 mW cm^{-2}. c,d) The energy band diagrams of (c) an open-circuited and (d) a short-circuited CdS:Ga NR/Au Schottky junction device under light illumination. Reproduced with permission.[179] Copyright 2012, Royal Society of Chemistry.

3.2.3. Self-Powered Photodetector Based on a Semiconductor/Graphene Nanostructure

In comparison to the p–n junction, the Schottky junction has the advantages of material universality, facile fabrication processes, etc. However, the remarkable light absorption of metals may seriously limit the performance of the PDs made from a Schottky junction. Graphene, an atomic-layer-thick and two-dimensional system,[180] has triggered considerable research interest due to its fascinating electronic and mechanic properties prescribed by its unique structure.[181–186]

Graphene, as a substitute for metal, was used to fabricate the self-powered visible-light PD based on a CdSe NB/graphene junction (**Figure 12**a).[187] Under zero bias, such PD typically shows a high photosensitivity (~3.5×10^5) to above-bandgap irradiation and a fast response (with response and recovery times of 82 μs and 179 μs, respectively) in a wide range of switching frequencies (up to 1000 Hz) (Figure 12b). The mechanism of the self-powered PD can be explained qualitatively as follows: because of the work function difference between the two materials, a built-in electric field forms between graphene and the CdSe NB. Upon above-bandgap light illumination, the photogenerated holes and electrons are driven towards the graphene and the CdSe NB, respectively, by the built-in field. The offset between the quasi-Fermi levels of the CdSe NB and graphene results from the voltage drop on the external load, which is analogous to applying a forward bias to the junction (Figure 12c). This kind of high performance PD, with the advantages of easy fabrication and energy saving, shows wide application potential in the fields of visible-light detection, binary switches, and optoelectronic integrated circuits.

On the other hand, the optical and electronic properties of semiconductor nanoparticles (NPs) can be tuned by the size, shape,

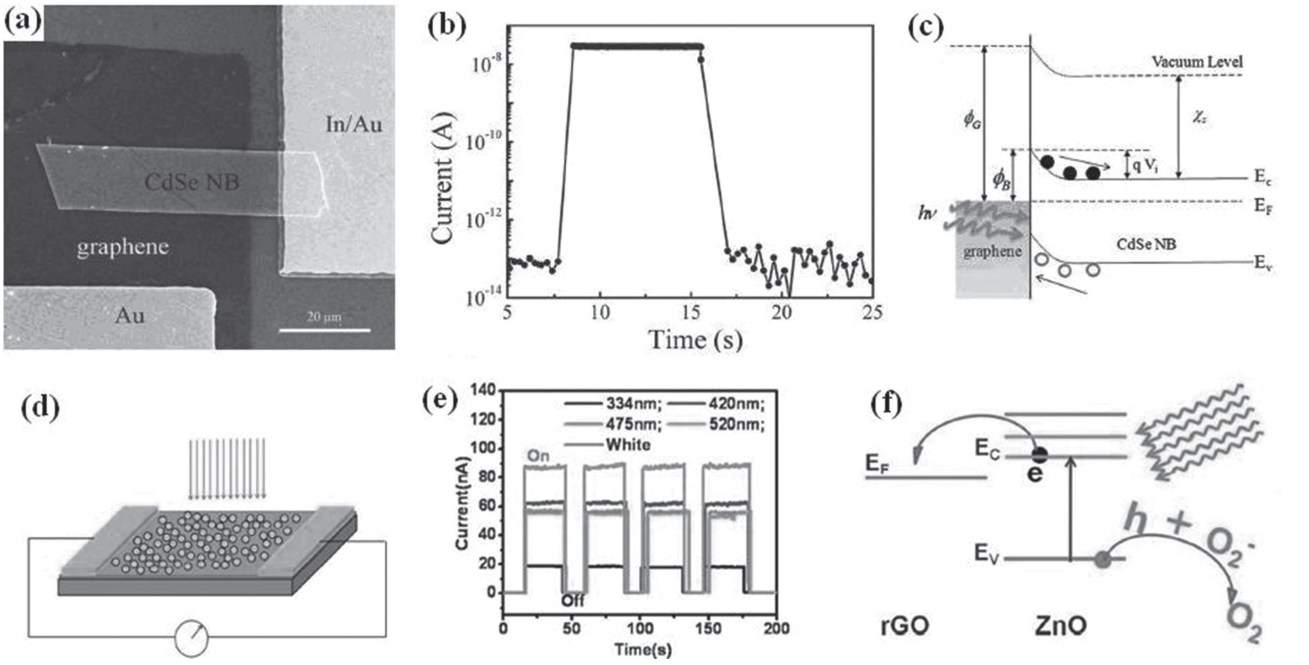

Figure 12. a) FESEM image of the photodetector. b) Photocurrent response measured at zero bias (under short circuit conditions) under a fixed white light illumination. c) The energy band diagrams of such photodetector under light illumination for the load (resistor) cases. Φ_G is the work function of graphene, Φ_B is the Schottky barrier height, V_i is the built-in potential, V is the voltage drop on the resistor, χ_S is the electron affinity of the CdSe NB. E_C, E_V, and E_F are the conduction band edge, valence band edge, and Fermi level of the CdSe NB, respectively. Reproduced with permission.[187] Copyright 2012, Royal Society of Chemistry. d) Schematic illustration of ZnO decorated rGO-ZnO composite PD. e) Time-resolved photocurrent generation with illumination for the rGO–ZnO PD. f) Schematic illustration of charge transfer process involving oxygen-adsorption upon illumination of carbon-doped ZnO–rGO hybrid, the brown lines denote new energy levels generated by carbon doping. Reproduced with permission.[195] Copyright 2012, Royal Society of Chemistry.

and composition.[188,189] Thus it is of great interest to modify graphene sheets with such semiconductor NPs, because the combination of certain NPs with graphene might produce promising optoelectronic and energy-conversion materials. For example, a reduced graphene oxide (rGO)-semiconductor NP nanocomposite with interesting photovoltaic response and improved photoinduced charge-transfer properties[190,191] has been synthesized; an rGO-CdSe hybrid shows dramatically enhanced photoresponse.[192] In these materials, the excited electrons in the conduction band of semiconductor NPs will migrate into rGO, thereby decreasing the recombination possibility of electron–hole pairs. Meanwhile, countless endeavours have been devoted to extending the absorption of ZnO from the UV band to the visible zone. Various strategies, including atomic doping and surface modification by heterogeneous species, have been proposed to enhance the absorption of ZnO in the visible band.[193,194] In particular, a carbon-doping method has been widely used to enhance the visible-light absorption of ZnO and improve its visible-light photocatalytic activity;[193] rGO was also used to enhance the photocatalytic activity of ZnO NPs.[194] Recently, a rGO-ZnO NPs nanocomposite PD with ultrasensitive visible-light photoresponse has been synthesized (Figure 12d) and could produce a distinct electric current to visible-light illumination under zero-bias, making the PD self-powered.[195] Under white-light illumination, the photoresponsivity defined by the ratio of photocurrent to dark current reached 430, and both rise and fall times are less than 0.2 s (Figure 12e). The mechanism of photoresponse is different from those for the graphene photodetecting devices based on the Schottky junction.[196,197] The photocurrent in the self-powered PD comes from a synergic effect of rGO and ZnO: effective charge transfer between their interface and fast charge transport by rGO. When ambient oxygen molecules are adsorbed on ZnO surface, they capture the free electrons present in the n-type ZnO [$O_2(g)+e^- \rightarrow O_{\bar{2}}$ (ad)], generating a low-conductivity depletion layer near the surface. When the device is illuminated by photons with energy higher than the E_g of ZnO ($h\nu > E_g$), e–h pairs are photogenerated ($h\nu \rightarrow e^- + h^+$) in ZnO NPs. The photogenerated holes will migrate to the ZnO surface and combine with oxygen [$O_{\bar{2}}$ (ad)$+h^+ \rightarrow O_2(g)$], while free electrons will be transferred into the rGO layer the built-in field within the depletion region and then transported to the electrode. Further, the rGO-ZnO hybrid introduces narrow energy levels in the forbidden gap of the carbon-doped ZnO and extends the absorption from the UV zone to the visible zone, thus a distinct photocurrent is generated under zero bias (Figure 12e).

4. Summary and Outlook

As a new field in self-powered nanotechnology-related research, self-powered PDs have been developed, which exhibit a much faster photoresponse and higher photosensitivity than the conventional photoconductor-based PDs and show potential applications in light detecting and nano-optoelectronic integrated circuits. The decisive factor for the implementation of

self-powered PDs is the successful development of energy-harvesting devices to provide appropriate power sources that can sustainably and stably operate over a broad range of conditions. For comparison, the major energy-harvesting techniques discussed herein and their prospects for application in self-powered PDs are summarized in Table 1 and Table 2, respectively.

Despite the rapid progress that has been made in the new field of self-powered PDs, the practical applications still require the development of the much higher performance self-powered PDs. Therefore, considerable future study of fabrication of self-powered PDs is proposed. First, power-source devices with more stable and sufficiently high outputs are still needed to power the self-powered PDs. Although some self-powered PDs, such as the self-powered PD integrated a single-fiber NW hybrid-structured MFC,[168] show an excellent response and photosensitivity to solar light, the highest photocurrent value is only in the region of 10^{-9}~10^{-8} A, which is very low and difficult for it to meet the requirements of practical applications. Second, the detection performance of PD itself needs to be further improved. Many PDs indicate that the limitation of the detectable light intensity is very high. However, for environmental monitoring and medical therapy treatment, weak light detection is much more desired. For instance, a rapid and high-sensitive PD is urgently required to detect fluorescence of the contamination in recycled water systems for environmental monitoring.[44,45] In addition, innovative approaches should be developed to greatly reduce the size and weight of self-powered systems, especially for implanted biomedical systems. When these issues are addressed properly, sustainable self-powered PDs will play a critical role in the advancement of the important fields of imaging techniques, light-wave communications, environmental monitoring, medical science, defense technology, and so on

In summary, the development of self-powered PDs requires the rational synthesis of nanomaterials, measurements of nanoscale properties, fabrication of nanodevices, integration of various nanodevices into systems with multi-functionality, and harvesting energy to power the self-powered system. We look forward to seeing a marked impact of self-powered nanotechnology on nanostructural PDs. The fabricated self-powered PDs will be intelligent, multifunctional, super-small, extremely sensitive, and energy efficient in the near future. The development of the self-powered PDs should also open up other novel research areas and challenging techniques.

Acknowledgments

This work was supported by the Postdoctoral Science Foundation of China (2012M520825), the National Natural Science Foundation of China (Grant Nos. 91123006, 51372040 and 51002032), Shanghai Shu Guang Project (12SG01), Shanghai Pujiang Program (11PJ1400300, 12PJ1400300), Innovation Program of Shanghai Municipal Education Commission (14ZZ003), Science and Technology Commission of Shanghai Municipality (13NM1400300 and 11520706200), the Programs for Professor of Special Appointment (Eastern Scholar) at Shanghai Institutions of Higher Learning and for New Century Excellent Talents in University (NCET-11–0102) and the National Basic Research Program of China (Grant No. 2012CB932303).

Received: September 30, 2013
Revised: November 3, 2013
Published online: January 14, 2014

[1] Z. L. Wang, J. H. Song, *Science* **2006**, *312*, 242.
[2] C. Z. Yuan, J. Y. Li, L. R. Hou, X. G. Zhang, L. F. Shen, X. W. Lou, *Adv. Funct. Mater.* **2012**, *22*, 4592.
[3] Z. L. Wang, Nanogenerators for Self-Powered Devices and Systems, Georgia Institute of Technology, http://smartech.gatech.edu/handle/1853/39262, accessed: June, 2011.
[4] Y. Q. Bie, Z. M. Liao, H. Z. Zhang, G. R. Li, Y. Ye, Y. B. Zhou, J. Xu, Z. X. Qin, L. Dai, D. P. Yu, *Adv. Mater.* **2011**, *23*, 649.
[5] Z. L. Wang, *Adv. Mater.* **2012**, *24*, 280.
[6] F. Zhang, C. Z. Yuan, J. J. Zhu, J. Wang, X. G. Zhang, X. W. Lou, *Adv. Funct. Mater.* **2013**, *23*, 3909.
[7] X. S. Fang, T. Y. Zhai, U. K. Gautam, L. Li, L. M. Wu, Y. Bando, D. Golberg, *Prog. Mater. Sci.* **2011**, *56*, 175.
[8] Y. Hu, Y. Zhang, C. Xu, G. Zhu, Z. L. Wang, *Nano Lett.* **2010**, *12*, 5025.
[9] J. Han, F. Fan, C. Xu, S. Lin, M. Wei, X. Duan, Z. L. Wang, *Nanotechnology* **2010**, *21*, 405203.
[10] Y. Hu, C. Xu, Y. Zhang, L. Lin, R. L. Snyder, Z. L. Wang, *Adv. Mater.* **2011**, *23*, 4068.
[11] M. Lee, J. Bae, J. Lee, C. S. Lee, S. Hong, Z. L. Wang, *Energy Environ. Sci.* **2011**, *9*, 3359.
[12] H. Zhang, K. Yeung, J. S. Robbins, R. A. Pavlick, M. Wu, R. Liu, A. Sen, S. T. Phillips, *Angew. Chem. Int. Ed.* **2012**, *51*, 2400.
[13] R. Dahal, K. C. Huang, J. Clinton, N. LiCausi, J.-Q. Lu, Y. Danon, I. Bhat, *Appl. Phys.Lett.* **2012**, *100*, 243507.
[14] Z. L. Wang, *Adv. Funct. Mater.* **2008**, *18*, 3553.
[15] Z. Bai, X. Yan, X. Chen, H. Liu, Y. Shen, Y. Zhang, *Curr. Appl. Phys.* **2013**, *13*, 165.
[16] A. Yu, P. Jiang, Z. L. Wang, *Nano Energy* **2012**, *1*, 418.
[17] X. Li, C. Gao, H. Duan, B. Lu, X. Pan, E. Xie, *Nano Energy* **2012**, *1*, 640.
[18] M. Chen, L. F. Hu, J. X. Xu, M. Y. Liao, L. M. Wu, X. S. Fang, *Small* **2011**, *7*, 2449.
[19] H. Kind, H. Q. Yan, B. Messer, M. Law, P. D. Yang, *Adv. Mater.* **2002**, *14*, 158.
[20] X. S. Fang, L. M. Wu, L. F. Hu, *Adv. Mater.* **2011**, *23*, 585.
[21] L. F. Hu, M. M. Brewster, X. J. Xu, C. C. Tang, S. Gradečak, X. S. Fang, *Nano Lett.* **2013**, *12*, 1941.
[22] P. C. Wu, Y. Dai, Y. Ye, Y. Yin, L. Dai, *J. Mater. Chem.* **2011**, *21*, 2563.
[23] T. Y. Zhai, L. Li, X. Wang, X. S. Fang, Y. Bando, D. Golberg, *Adv. Funct. Mater.* **2010**, *20*, 4233.
[24] Y. Jiang, W. J. Zhang, J. S. Jie, X. M. Meng, X. Fan, S. T. Lee, *Adv. Funct. Mater.* **2007**, *17*, 1795.
[25] J. S. Jie, W. J. Zhang, Y. Jiang, X. M. Meng, Y. Q. Li, S. T. Lee, *Nano Lett.* **2006**, *6*, 1887.
[26] L. B. Luo, X. B. Yang, F. X. Liang, J. S. Jie, Q. Li, Z. F. Zhu, C. Y. Wu, Y. Q. Yu, L. Wang, *CrystEngComm* **2012**, *14*, 1942.
[27] T. Y. Wei, C. T. Huang, B. J. Hansen, Y. F. Lin, L. J. Chen, S. Y. Lu, Z. L. Wang, *Appl. Phys. Lett.* **2010**, *96*, 013508.
[28] T. Y. Zhai, L. Li, Y. Ma, M. Y. Liao, X. Wang, X. S. Fang, J. N. Yao, Y. Bando, D. Golberg, *Chem. Soc. Rev.* **2011**, *40*, 2986.
[29] Y. Q. Yu, J. S. Jie, P. Jiang, L. Wang, C. Y. Wu, Q. Peng, X. W. Zhang, Z. Wang, C. Xie, D. Wu, Y. Jiang, *J. Mater. Chem.* **2011**, *21*, 12632.
[30] C. Y. Wu, J. S. Jie, L. Wang, Y. Q. Yu, Q. Peng, X. W. Zhang, J. J. Cai, H. E. Guo, D. Wu, Y. Jiang, *Nanotechnology* **2010**, *21*, 505203.
[31] P. C. Wu, Y. Dai, T. Sun, Y. Ye, H. Meng, X. L. Fang, B. Yu, L. Dai, *ACS Appl. Mater. Interfaces* **2011**, *3*, 1859.
[32] C. S. Lao, M. C. Park, Q. Kuang, Y. L. Deng, A. K. Sood, P. L. Polla, Z. L. Wang, *J. Am. Chem. Soc.* **2007**, *129*, 12096.
[33] J. Z. Zhou, L. L. Lin, L. J. Zhang, Z. H. Lin, *J. Phys. Chem. C* **2011**, *115*, 16828.
[34] J. M. Wu, C. H. Kuo, *Thin Solid Films* **2009**, *517*, 3870.
[35] A. Yamakata, M. Yoshida, J. Kubotu, M. Osawa, K. Domen, *J.Am. Chem. Soc.* **2011**, *133*, 11351.

[36] H. Wu, Y. Sun, D. Lin, R. Zhong, C. Zhang, W. Pan, *Adv. Mater.* **2009**, *21*, 227.
[37] X. S. Fang, Y. Bando, M. Liao, U. Gautam, C. Zhi, B. Dierne, B. Liu, T. Zhai, T. Sekiguchi, Y. Koide, D. Golberg, *Adv. Mater.* **2009**, *21*, 2034.
[38] X. S. Fang, L. Hu, K. Huo, B. Gao, L. Zhao, M. Liao, P. Chu, Y. Bando, D. Golberg, *Adv. Funct. Mater.* **2011**, *21*, 3907.
[39] X. S. Fang, S. L. Xiong, T. Y. Zhai, Y. Bando, M. Y. Liao, U. K. Gautam, Y. Koide, X. G. Zhang, Y. T. Qian, D. Golberg, *Adv. Mater.* **2009**, *21*, 5016.
[40] R. R. Prabhakar, N. Mathews, K. B. Jinesh, K. R. G. Karthik, S. S. Pramana, B. Varghese, C. H. Sow, S. Mhaisalkar, *J. Mater. Chem.* **2012**, *22*, 9678.
[41] L. F. Hu, J. Yan, M. Y. Liao, H. J. Xiang, X. G. Gong, L. D. Zhang, X. S. Fang, *Adv. Mater.* **2012**, *24*, 2305.
[42] S. Xu, Y. Qin, C. Xu, Y. Wei, R. Yang, Z. L. Wang, *Nat. Nanotechnol.* **2010**, *5*, 366.
[43] Y. Yang, W. Guo, J. J. Qi, J. Zhao, Y. Zhang, *Appl. Phys. Lett.* **2010**, *97*, 223113.
[44] R. K. Henderson, A. Baker, K. R. Murphy, A. Hambly, R. M. Stuetz, S. J. Khan, *Water Res.* **2009**, *43*, 863.
[45] M. A. Shannon, P. W. Bohn, M. Elimelech, J. G. Georgiadis, B. J. Marinas, A. M. Mayes, *Nature* **2008**, *452*, 301.
[46] Y. Hu, Y. Zhang, C. Xu, L. Lin, R. L. Snyder, Z. L. Wang, *Nano Lett.* **2011**, *11*, 2572.
[47] X. Yang, G. Zhu, S. Wang, R. Zhang, L. Lin, W. Wua, Z. L. Wang, *Energy Environ. Sci.* **2012**, *5*, 9462.
[48] B. Yian, X. Zheng, T. J. Kempa, Y. Fang, N. Yu, G. Yu, J. Huang, C. M. Lieber, *Nature* **2007**, *449*, 885.
[49] Y. Ye, L. Dai, P. C. Wu, C. Liu, T. Sun, R. M. Ma, G. G. Qin, *Nanotechnology* **2009**, *20*, 375202.
[50] S. Yoo, B. Domercq, B. Kippelen, *Appl. Phys. Lett.* **2004**, *85*, 5427.
[51] A. L. Briseno, T. W. Holcombe, A. I. Boukai, E. C. Garnett, S. W. Shelton, J. J. M. Frechet, P. D. Yang, *Nano Lett.* **2010**, *10*, 334.
[52] K. Y. Lee, B. Kumar, J. Seo, K. Kim, J. I. Sohn, S. N. Cha, D. Choi, Z. L. Wang, S. Kim, *Nano Lett.* **2012**, *12*, 1959.
[53] M. Minary-Jolandan, R. A. Bernal, I. Kuljanishvili, V. Parpoil, H. D. Espinosa, *Nano Lett.* **2012**, *12*, 970.
[54] M. Zhou, N. Zhou, F. Kuralay, J. R. Windmiller, S. Parkhomovsky, G. Valdés, E. Katz, J. Wang, *Angew. Chem. Int. Ed.* **2012**, *51*, 2686.
[55] C. Xu, X. D. Wang, Z. L. Wang, *J. Am. Chem. Soc.* **2009**, *131*, 5866.
[56] X. Z. Guo, Y. D. Zhang, D. Qin, Y. H. Luo, D. M. Li, Y. T. Pang, Q. B. Meng, *J. Power Sources* **2010**, *195*, 7684.
[57] M. Lee, R. Yang, C. Li, Z. L. Wang, *J. Phys. Chem. Lett.* **2010**, *1*, 2929.
[58] Y. Yang, H. Zhang, G. Zhu, S. Lee, Z. Lin, Z. L. Wang, *ACS Nano* **2013**, *7*, 785.
[59] A. J. Baca, M. A. Meitl, H. C. Ko, S. Mack, H.-S. Kim, J. Y. Dong, P. M. Ferreira, J. A. Rogers, *Adv. Funct. Mater.* **2007**, *17*, 3051.
[60] J. S. Jie, W. J. Zhang, K. Q. Peng, G. D. Yuan, C. S. Lee, S. T. Lee, *Adv. Funct. Mater.* **2008**, *18*, 3251.
[61] Y. H. Kwon, S. W. Woo, H. R. Jung, H. K. Yu, K. Kim, B. H. Oh, A. Ahn, S. Y. Lee, S. W. Song, J. Cho, H. C. Shin, J. Y. Kim, *Adv. Mater.* **2012**, *24*, 5192.
[62] Y. Ke, X. Wang, X. J. Weng, C. E. Kendrick, Y. A. Yu, S. M. Eichfeld, H. P. Yoon, J. M. Redwing, T. S. Mayer, Y. M. Habib, *Nanotechnology* **2011**, *22*, 445401.
[63] a)T. J. Kempa, B. Z. Tian, D. R. Kim, J. S. Hu, X. L. Zheng, C. M. Lieber, *Nano Lett.* **2008**, *8*, 3456; b) B. Z. Tian, X. L. Zheng, T. J. Kempa, Y. Fang, N. F. Yu, G. H. Yu, J. L. Huang, C. M. Lieber, *Nature* **2007**, *449*, 885.
[64] P. Chiu, S. Wojtczuk, X. Zhang, C. Harris, D. Pulver, M. Timmons, *37th IEEE Photovoitaic Specialists Conference (PVSC)* **2011**, 771–774.
[65] M. D. Kelzenberg, D. B. Turner-Evans, B. M. Kayes, M. A. Filler, M. C. Putnam, N. S. Lewis, H. A. Atwater, *Nano Lett.* **2008**, *8*, 710.
[66] J. D. Kim, J.-H. Yun, C.-S. Han, Y. J. Cho, J. H. Park, Y. C. Park, *Appl. Phys. Lett.* **2009**, *95*, 143112.
[67] K. S. Novoselov, A. K. Geim, S. V. Morozov, D. Jiang, Y. Zhang, S. V. Dubonos, I. V. Grigorieva, A. A. Firsov, *Science* **2004**, *306*, 666.
[68] S. P. Pang, Y. Hernandez, X. L. Feng, K. Mullen, *Adv. Mater.* **2011**, *23*, 2779.
[69] C. X. Guo, G. H. Guai, C. M. Li, *Adv. Energy Mater.* **2011**, *1*, 448.
[70] Y. Ye, L. Gan, L. Dai, Y. Dai, X. F. Guo, H. Meng, B. Yu, Z. J. Shi, K. P. Shang, G. G. Qin, *Nanoscale* **2011**, *3*, 1477.
[71] C. Xie, J. Jie, B. Nie, T. Yan, Q. Li, P. Lv, F. Li, M. Wang, C. Wu, L. Wang, L. Luo, *Appl. Phys. Lett.* **2012**, *100*, 193103.
[72] Y. Ye, Y. Dai, L. Dai, Z. J. Shi, N. Liu, F. Wang, L. Fu, R. M. Peng, X. N. Wen, Z. J. Chen, Z. F. Liu, G. G. Qin, *ACS Appl. Mater. Interfaces* **2010**, *2*, 3406.
[73] X. M. Li, H. W. Zhu, K. L. Wang, A. Y. Cao, J. Q. Wei, C. Y. Li, Y. Jia, Z. Li, X. Li, D. H. Wu, *Adv. Mater.* **2010**, *22*, 2743.
[74] G. F. Fan, H. W. Zhu, K. L. Wang, J. Q. Wei, X. M. Li, Q. K. Shu, N. Guo, D. H. Wu, *ACS Appl. Mater. Interfaces* **2011**, *3*, 721.
[75] C. Xie, P. Lv, B. Nie, J. S. Jie, X. W. Zhang, Z. Wang, P. Jiang, Z. Z. Hu, L. B. Luo, Z. F. Zhu, L. Wang, C. Y. Wu, *Appl. Phys. Lett.* **2011**, *99*, 133113.
[76] Z. Li, H. W. Zhu, D. Xie, K. L. Wang, A. Y. Cao, J. Q. Wei, X. Li, L. L. Fan, D. H. Wu, *Chem. Commun.* **2011**, *47*, 3520.
[77] J. Grönqvist, N. Søndergaard, F. Boxberg, T. Guhr, S. Åberg, H. Q. Xu, *J. Appl. Phys.* **2009**, *106*, 53508.
[78] N. Søndergaard, Y. He, C. Fan, R. Han, T. Guhr, H. Q. Xu, *J. Vac. Sci. Technol. B* **2009**, *27*, 827.
[79] F. Boxberg, N. Søndergaard, H. Q. Xu, *Nano Lett.* **2010**, *10*, 1108.
[80] Z. L. Wang, *Adv. Mater.* **2012**, *24*, 4632.
[81] C. Pan, S. Niu, Y. Ding, L. Dong, R. Yu, Ying. Liu, G. Zhu, Z. L. Wang, *Nano Lett.* **2012**, *12*, 3302.
[82] S. N. Cha, S. M. Kim, H. J. Kim, J. Y. Ku, J. I. Sohn, Y. J. Park, B. G. Song, M. H. Jung, E. K. Lee, B. L. Choi, J. J. Park, Z. L. Wang, J. M. Kim, K. Kim, *Nano Lett.* **2011**, *11*, 5142.
[83] C. L. Sun, J. Shi, D. J. Bayerl, X. D. Wang, *Energy Environ. Sci.* **2011**, *4*, 4508.
[84] Z. T. Li, Z. L. Wang, *Adv. Mater.* **2011**, *23*, 84.
[85] Y. F. Hu, L. Lin, Y. Zhang, Z. L. Wang, *Adv. Mater.* **2012**, *24*, 110.
[86] S. Xu, B. J. Hansen, Z. L. Wang, *Nat. Commun.* **2010**, *1*, 93.
[87] X. Wang, J. Song, J. Liu, Z. L. Wang, *Science* **2007**, *316*, 102.
[88] G. Zhu, R. Yang, S. Wang, Z. L. Wang, *Nano Lett.* **2010**, *10*, 3151.
[89] F. R. Fan, Z. Q. Tian, Z. L. Wang, *Nano Energy* **2012**, *1*, 328.
[90] G. Zhu, C. Pan, W. Guo, C.-Y. Chen, Y. Zhou, R. Yu, Z. L. Wang, *Nano Lett.* **2012**, *12*, 4960.
[91] Y. Yang, W. Guo, K. C. Pradel, G. Zhu, Y. Zhou, Y. Zhang, Y. Hu, L. Lin, Z. L. Wang, *Nano Lett.* **2012**, *12*, 2833.
[92] Y. Yang, J. H. Jung, B. K. Yun, F. Zhang, K. C. Pradel, W. Guo, Z. L. Wang, *Adv. Mater.* **2012**, *24*, 5357.
[93] R. Zhang, L. Lin, Q. Jing, W. Wu, Y. Zhang, Z. Jiao, L. Yan, R. P. S. Han, Z. L. Wang, *Energy Environ. Sci.* **2012**, *5*, 8528.
[94] A. Yu, P. Jiang, Z. L. Wang, *Nano Energy* **2012**, *1*, 418.
[95] L. Lin, Y. Hu, C. Xu, Y. Zhang, R. Zhang, X. Wen, Z. L. Wang, *Nano Energy* **2013**, *2*, 75.
[96] X. D. Wang, J. Zhou, J. H. Song, J. Liu, N. S. Xu, Z. L. Wang, *Nano Lett.* **2006**, *6*, 2768.
[97] J. H. He, C. L. Hsin, J. Liu, L. J. Chen, Z. L. Wang, *Adv. Mater.* **2007**, *19*, 781.
[98] Z. L. Wang, *Adv. Mater.* **2007**, *19*, 889.
[99] Z. L. Wang, R. S. Yang, J. Zhou, Y. Qin, C. Xu, Y. F. Hu, S. Xu, *Mater. Sci. Eng.* **2010**, *R70*, 320.
[100] R. S. Yang, Y. Qin, L. M. Dai, Z. L. Wang, *Nat. Nanotechnol.* **2009**, *4*, 34.
[101] C. T. Huang, J. H. Song, C. M. Tsai, W. F. Lee, D. H. Lien, Z. Y. Gao, Y. Hao, L. J. Chen, Z. L. Wang, *Adv. Mater.* **2010**, *22*, 4008.

[102] M. Y. Lu, J. H. Song, M. P. Lu, C. Y. Lee, L. J. Chen, Z. L. Wang, *ACS Nano* **2009**, *3*, 357.
[103] X. Chen, S. Y. Xu, N. Yao, Y. Shi, *Nano Lett.* **2010**, *10*, 2133.
[104] X. Y. Zhang, X. Zhao, C. W. Lai, J. Wang, X. G. Tang, J. Y. Dai, *Appl. Phys. Lett.* **2004**, *85*, 4190.
[105] C. Chen, G. Zhu, Y. Hu, J. Yu, J. Song, K. Cheng, L. Peng, L. Chou, Z. L. Wang, *ACS Nano* **2012**; *6*, 5687.
[106] Y. Qi, N. T. Jafferis, K. Lyons, C.M. Lee, H. Ahmad, M. C. McAlpine, *Nano Lett.* **2010**, *10*, 524.
[107] K. I. Park, S. Xu, Y. Liu, G.-T. Hwang, S.-J. L. Kang, Z. L. Wang, K. J. Lee, *Nano Lett.* **2010**, *10*, 4939.
[108] C. Sun, J. Shi, D. J. Bayerl, X. Wang, *Energy Environ. Sci.* **2011**, *4*, 4508.
[109] J. Fang, X. G. Wang, T. J. Lin, *Mater. Chem.* **2011**, *21*, 11088.
[110] C. E. Chang, V.H. Tran, J. B. Wang, Y. K. Fuh, L. W. Lin, *Nano Lett.* **2010**, *10*, 726.
[111] A. Dorfman, N. Kumar, J. I. Hahm, *Langmuir* **2006**, *22*, 4890.
[112] Z. Y. Fan, D. W. Wang, P. C. Chang, W. Y. Tseng, J. G. Lu, *Appl. Phys. Lett.* **2004**, *85*, 5923.
[113] Y. Qin, X. D. Wang, Z. L. Wang, *Nature* **2008**, *451*, 809.
[114] X. Chen, S. Y. Xu, N. Yao, W. H. Xu, Y. Shi, *Appl. Phys. Lett.* **2009**, *94*, 253113.
[115] Z. Y. Wang, J. Hu, A. P. Suryavanshi, K. Yum, M. F. Yu, *Nano Lett.* **2007**, *7*, 2966.
[116] Y. Qi, J. Kim, T. D. Nguyen, B. Lisko, P. K. Purohit, M. C. McAlpine, *Nano Lett.* **2011**, *11*, 1331.
[117] W. Wu, S. Bai, M. Yuan, Y. Qin, Z. L. Wang, T. Jing, *ACS Nano* **2012**, *6*, 6231.
[118] J. Kwom, W. Seung, B. K. Sharma, S. Kim, J. Ahn, *Energy Environ. Sci.* **2012**, *5*, 8970.
[119] F. R. Fan, Z. Q. Tian, Z. L. Wang, *Nano Energy* **2012**, *1*, 328.
[120] F. R. Fan, L. Lin, G. Zhu, W. Wu, R. Zhang, Z. L. Wang, *Nano Lett.* **2012**, *12*, 3109.
[121] F. J. DiSalvo, *Science* **1999**, *285*, 703.
[122] L. E. Bell, *Science* **2008**, *321*, 1457.
[123] X. Yan, B. Poudel, Y. Ma, Liu, S. W. G. Joshi, H. Wang, Y. C. Lan, D. Z. Wang, G. Chen, Z. F. Ren, *Nano Lett.* **2010**, *10*, 3373.
[124] Y. Zhang, M. S. Dresselhaus, Y. Shi, Z. Ren, G. High, *Chen Nano Lett.* **2011**, *11*, 1166.
[125] M. Zebarjadi, K. Esfarjani, M. S. Dresselhaus, Z. F. Ren, G. Chen, *Energy Environ. Sci.* **2012**, *5*, 5147.
[126] G. Sebald, D. Guyomar, A. Agbossou, *Smart Mater. Struct.* **2009**, *18*, 125006.
[127] R. S. Thompson, D. Li, C. M. Witte, J. G. Lu, *Nano Lett.* **2009**, *9*, 3991.
[128] Y. Yang, J. Qi, Q. Liao, Y. Zhang, L. Tang, Z. Qin, *J. Phys. Chem. C* **2008**, *112*, 17916.
[129] Y. Yang, K. Pradel, Q. Jing, J. Wu, F. Zhang, Y. Zhou, Y. Zhang, Z. L. Wang, *ACS Nano* **2012**, *6*, 6984.
[130] Y. Yang, Y. Zhou, J. Wu, Z. L. Wang, *ACS Nano* **2012**, *6*, 8456.
[131] M. Zhou, J. Wang, *Electroanalysis* **2012**, *24*, 197.
[132] C. Pan, H. Wu, C. Wang, B. Wang, L. Zhang, Z. Cheng, P. Hu, W. Pan, Z. Zhou, X , Yang, J. Zhu, *Adv. Mater.* **2008**, *20*, 1644.
[133] R. R. Harrison, C. Koch, *Analog. Integr. Circ. S.* **2000**, *24*, 213.
[134] C. Pan, Y. Yang, H. Wu, M. Ahmad, Z. Luo, Q. Li, J. Xie, X. Yan, L. Wu, Z. L. Wang, J. Zhu, *Adv. Mater.* **2010**, *22*, 5388.
[135] J. Zhou, N. S. Xu, Z. L. Wang, *Adv. Mater.* **2006**, *18*, 2432.
[136] C. Xu, C. Pan, Y. Liu, Z. L. Wang, *Nano Energy* **2012**, *1*, 259.
[137] C. Xu, Z. L. Wang, *Adv. Mater.* **2011**, *23*, 873.
[138] D. Choi, K. Y. Lee, M. J. Jin, S. G. Ihn, S. Yun, X. Bulliard, W. Choi, S. Y. Lee, S. W. Kim, J. Y. Choi, J. M. Kim, Z. L. Wang, *Energy Environ. Sci.* **2011**, *4*, 4607.
[139] C. F. Pan, Z. T. Li, W. X. Guo, J. Zhu, Z. L. Wang, *Angew. Chem., Int. Ed.* **2011**, *50*, 11192.
[140] B. J. Hansen, Y. Liu, R. S. Yang, Z. L. Wang, *ACS Nano* **2010**, *4*, 3647.
[141] C. Pan, W. Guo, L. Dong, G. Zhu, Z. L. Wang, *Adv. Mater.* **2012**, *24*, 3356.
[142] B. Weintraub, Y. G. Wei, Z. L. Wang, *Angew. Chem., Int. Ed.* **2009**, *48*, 8981.
[143] D. N. Futaba, K. Hata, T. Yamada, T. Hiraoka, Y. Hayamizu, Y. Kakudate, O. Tanaike, H. Hatori, M. Yumura, S. Iijima, *Nat Mater.* **2006**, *5*, 987.
[144] J. Chmiola, C. Largeot, P. L. Taberna, P. Simon, Y. Gogotsi, *Science* **2010**, *328*, 480.
[145] C. K. Chan, H. L. Peng, G. Liu, K. McIlwrath, X. F. Zhang, R. A. Huggins, Y. Cui, *Nat. Nanotechnol.* **2008**, *3*, 31.
[146] P. Poizot, S. Laruelle, S. Grugeon, L. Dupont, J. M. Tarascon, *Nature* **2000**, *407*, 496.
[147] J. M. Miller, B. Dunn, T. D. Tran, R.W. Pekala, *J. Electrochem. Soc.* **1997**, *144*, L309.
[148] B. E. Conway, Electrochemical Supercapacitors: Scientific, Fundamentals and Technological Applications, Plenum, New York **1999**, pp. 29–30.
[149] E. Frackowiak, F. Beguin, *Carbon* **2001**, *39*, 937.
[150] R. Kötz, M. Carlen, *Electrochim. Acta* **2000**, *45*, 2483.
[151] J. R. Miller, P. Simon, *Science* **2008**, *321*, 651.
[152] C. Meng, C. Liu, L. Chen, C. Hu, S. Fan, *Nano Lett.* **2010**, *10*, 4025.
[153] M. Kaempgen, C. K. Chan, J. Ma, Y. Cui, G. Gruner, *Nano Lett.* **2009**, *9*, 1872.
[154] Z. Weng, Y. Su, D.-W. Wang, F. Li, J. Du, H.-M. Cheng, *Adv. Energ. Mater.* **2011**, *1*, 917.
[155] L. Yuan, X. Xiao, T. Ding, J. Zhong, X. Zhang, Y. Shen, B. Hu,Y. Huang , J. Zhou, Z. L. Wang, *Angew. Chem. Int. Ed.* **2012**, *51*, 4934.
[156] D. Pech, M. Brunet, H. Durou, P. Huang, V. Mochalin, Y. Gogotsi, P. L. Taberna, P. Simon, *Nat. Nanotechnol.* **2010**, *5*, 651.
[157] X. Xiao, T. Li, P. Yang, Y. Gao, H. Jin, W. Ni, W. Zhan, X. Zhang, Y. Cao, J. Zhong, L. Gong, W. Yen, W. Mai, J. Chen, K. Huo, Y. Chueh, Z. L. Wang, J. Zhou, *ACS Nano* **2012**, *6*, 9200.
[158] G. R. Li, Z. L. Wang, F. L. Zheng, Y. N. Ou, Y. X. Tong, *J. Mater. Chem.* **2011**, *21*, 4217.
[159] M. S. Wu, Y. H. Ou, Y. P. Lin, *Electrochim. Acta* **2010**, *55*, 3240.
[160] X. H. Lu, T. Zhai, X. H. Zhang, Y. Q. Shen, L. Y. Yuan, B. Hu, L. Gong, J. Chen, Y. H. Gao, J. Zhou, Y. X. Tong, Z. L. Wang, *Adv. Mater.* **2012**, *24*, 938.
[161] W. Gao, N. Singh, L. Song, Z. Liu, A. L. M. Reddy, L. Ci, R. Vajtai, Q. Zhang, B. Wei, P. M. Ajayan, *Nat. Nanotechnol.* **2011**, *6*, 496.
[162] Y. Idota, T. Kubota, A. Matsufuji, Y. Maekawa, T. Miyasaka, *Science* **1997**, *276*, 1395.
[163] J. M. Tarascon, M. Armand, *Nature* **2001**, *414*, 359.
[164] P. G. Bruce, B. Scrosati, J. M. Tarascon, *Angew. Chem., Int. Ed.* **2008**, *47*, 2930.
[165] G. Armstrong, A. R. Armstrong, P. G. Bruce, P. Reale, B. Scrosati, *Adv. Mater.* **2006**, *18*, 2597.
[166] M. Wakihara, O. Yamamoto, Lithium Ion Batteries: Fundamentals and Performance (Ed: Kodansha), Wiley-VCH, Germany **1998**.
[167] X. Xue, S. Wang, W. Guo, Y. Zhang, Z. L. Wang, *Nano Lett.* **2012**, *12*, 5048.
[168] Q. Yang, Y. Liu, Z. Li, Z. Yang, X. Wang, Z. L. Wang, *Angew. Chem. Int. Ed.* **2012**, *51*, 6443.
[169] C. Chen, K. Wang, S. Tsai, H. Chien, S. Wu, *Jpn. J. Appl. Phys.* **2010**, *49*, 04DG06.
[170] M. M. Adachi, K. Wang, F. Chen, K. S. Karim, *Proc. SPIE-Int.Soc. Opt. Eng.* **2010**, 7622, 76224M.
[171] H. Cho, A. S. Zakirov, S. U. Yuldashev, C. W. Ahn, Y. K. Yeo, T. W. Kang, *Nanotechnology* **2012**, *23*, 115401.
[172] O. Lupan, G. Chai, L. Chow, G. A. Emelchenko, H. Heinrich, V. V. Ursaki, A. N. Gruzintsev, I. M. Tiginyanu, A. N. Redkin, *Phys. Status Solidi A* **2010**, *207*, 1735.
[173] S. Yang, J. Gong, Y. Deng, *J. Mater. Chem.* **2012**, *22*, 13899.

[174] H. Y. Ma, Y. Q. Luo, S. X. Yang, Y. W. Li, F. Cao, J. Gong, *J. Phys. Chem. C* **2011**, *115*, 12048.
[175] D. Wu, Y. Jiang, Y. G. Zhang, J. W. Li, Y. Q. Yu, Y. P. Zhang, Z. F. Zhu, L. Wang, C. Y. Wu, L. B. Luo, J. S. Jie, *J. Mater. Chem.* **2012**, *22*, 6206.
[176] D. Wu, Y. Jiang, S. Y. Li, F. Z. Li, J. W. Li, X. Z. Lan, Y. G. Zhang, C. Y. Wu, L. B. Luo, J. S. Jie, *Nanotechnology* **2011**, *22*, 405201.
[177] P. C. Wu, Y. Dai, T. Sun, Y. Ye, H. Meng, X. L. Fang, B. Yu, L. Dai, *ACS Appl. Mater. Interfaces* **2011**, *3*, 1859.
[178] Y. Ye, L. Dai, P. C. Wu, C. Liu, T. Sun, R. M. Ma, G. G. Qin, *Nanotechnology* **2009**, *20*, 375202.
[179] D. Wu, Y. Jiang, Y. Zhang, Y. Yu, Z. Zhu, X. Lan, F. Li, C. Wu, L. Wang, L. Luo, *J. Mater. Chem.* **2012**, *22*, 23272.
[180] C. Lee, X. D. Wei, J. W. Kysar, J. Hone, *Science* **2008**, *321*, 385.
[181] S. Stankovich, D. A. Dikin, G. H. B. Dommett, K. M. Kohlhaas, E. J. Zimney, E. A. Stach, R. D. Piner, S. T. Nguyen, R. S. Ruoff, *Nature* **2006**, *442*, 282.
[182] A. H. Castro Neto, F. Guinea, N. M. R. Peres, K. S. Novoselov, A. K. Geim, *Rev. Mod. Phys* **2009**, *81*, 109.
[183] J. D. Fowler, M. J. Allen, V. C. Tung, Y. Yang, R. B. Kaner, B. H. Weiller, *ACS Nano* **2009**, *3*, 301.
[184] H. Gwon, H. S. Kim, K. U. Lee, D. H. Seo, Y. C. Park, Y. S. Lee, B. T. Ahn, K. Kang, *Energy Environ. Sci.* **2011**, *4*, 1277.
[185] X. Wang, L. J. Zhi, K. Mullen, *Nano Lett.* **2008**, *8*, 323.
[186] T. Mueller, F. N. A. Xia, P. Avouris, *Nat. Photonics* **2010**, *4*, 297.
[187] W. Jin, Y. Ye, L. Gan, B. Yu, P. Wu. Y. Dai, H. Meng, X. Guo, L. Dai, *J. Mater. Chem.* **2012**, *22*, 2863.
[188] V. A. Fonoberov, A. A. Balandin, J. Nanoelectron, *Optoelectron.* **2006**, *1*, 19.
[189] C. B. Murray, D. J. Norris, M. G. Bawendi, *J. Am. Chem. Soc.* **1993**, *115*, 8706.
[190] P. Wang, T. F. Jiang, C. Z. Zhu, Y. M. Zhai, D. J. Wang, S. J. Dong, *Nano Res.* **2010**, *3*, 794.
[191] P. Wang, Y. M. Zhai, D. J. Wang, S. J. Dong, *Nanoscale* **2011**, *3*, 1640.
[192] Y. Lin, K. Zhang, W. F. Chen, Y. D. Liu, Z. G. Geng, J. Zeng, N. Pan, L. F. Yan, X. P. Wang, J. G. Hou, *ACS Nano* **2010**, *4*, 3033.
[193] S. Cho, J. W. Jang, J. S. Lee, K. H. Lee, *CrystEngComm* **2010**, *12*, 3929.
[194] T. G. Xu, L. W. Zhang, H. Y. Cheng, Y. F. Zhu, *Appl. Catal. B* **2011**, *101*, 382.
[195] Z. Zhan, L. Zheng, Y. Pan, G. Sun, L. Li, *J. Mater.Chem.* **2012**, *22*, 2589.
[196] F. N. Xia, T. Mueller, Y. M. Lin, A. Valdes-Garcia, P. Avouris, *Nat. Nanotechnol.* **2009**, *4*, 839.
[197] E. J. H. Lee, K. Balasubramanian, R. T. Weitz, M. Burghard, K. Kern, *Nat. Nanotechnol.* **2008**, *3*, 486.